

# Application of a surrogate model for condition monitoring of a digital twin gas turbine

Junqi Luan <sup>a</sup>, Shuying Li <sup>a</sup>, Yunpeng Cao <sup>a,\*</sup>, Chengzhong Gu <sup>b</sup>

<sup>a</sup> College of Power and Engineering, Harbin Engineering University, No.145 Nantong Street, PO.Box, Harbin, Heilongjiang 150001, China

<sup>b</sup> Unit 91663, No.33 Baotou Road, Shibei District, Qingdao, China

## ARTICLE INFO

**Keywords:**

Gas turbine  
Surrogate model  
Subspace tracking  
Digital twin  
Condition monitoring

## ABSTRACT

Condition monitoring technology plays a crucial role in ensuring the reliable operation of gas turbines. Digital twin has propelled condition monitoring research into a new phase. This paper established a surrogate model of gas turbines for condition monitoring based on Markov-projection approximation subspace tracking. Furthermore, it explores the application of surrogate model in developing digital twin for gas turbines. The study initially establishes a Markov matrix and acquires an observation vector, utilizing the framework of the linear model. Utilizing real-time measurement data of gas turbine, the signal subspace of the observation vector auto-correlation matrix is updated through the projection approximation subspace tracking. By aligning this signal subspace with the generalized observability matrix, the identification results of the surrogate model parameters are obtained online. Furthermore, a variable weight projection approximation subspace tracking method has been proposed to enhance the algorithm robustness. Simulation and real experiment demonstrate that the surrogate model output effectively tracks the real-time changes in gas turbine measurement data. When faults and degradation arise, condition monitoring can be achieved by analyzing the evolution of model parameters to obtain feedback information from the gas turbine. The proposed method maintains its robustness in the presence of impulsive noise. These features offer a novel approach for the development of gas turbine digital twin.

## 1. Introduction

Gas turbines have emerged as predominant power sources across aviation, marine, and electric power industry. Operating in harsh environments, gas turbines are prone to fouling, wear, and corrosion within their gas path structures, which consequently degrade their performance. Over time, such deterioration can precipitate significant accidents [1]. Hence, condition monitoring of gas turbines [2–4], including fault detection, performance assessment, and trend forecasting, has become a vital area of research. Condition monitoring ensures not only the efficiency, reliability, and safety of the gas turbines but also their economic viability. The advent of digital twin technology in recent years offers a new solution to these challenges, providing an innovative approach to proactive maintenance and operational optimization.

First introduced by Grieves in 2003, the concept of a digital twin was initially described as comprising three key components: physical entities and virtual spaces and the interconnection between the two. However, it wasn't until 2011, when NASA introduced

\* Corresponding author.

E-mail address: [caoyunpeng@hrbeu.edu.cn](mailto:caoyunpeng@hrbeu.edu.cn) (Y. Cao).

## Nomenclature

### Variables

<b>A</b>	system matrix
<b>B</b>	control matrix
<b>C</b>	output matrix
$d_m$	Mahalanobis distance
<i>Error</i>	model error
<b>D<sub>b</sub>, g<sub>b</sub>, q<sub>b</sub>, e<sub>b</sub>, σ<sub>t</sub></b>	intermediate variables in PAST method
<i>f</i>	Future time domain size
$\bar{H}_f$	I/O stack vector coefficient matrix
<i>j</i>	input dimension
<b>K</b>	Kalman filter gain
<i>m</i>	output dimension
<b>M</b>	Markov parameter matrix
<i>n</i>	model order
n1	low-pressure compressor speed
n2	high-pressure compressor speed
n3	power turbine speed
<i>p</i>	past time domain size
<i>P</i>	gas turbine power
P6	low-pressure turbine exhaust pressure
<b>Q<sub>k</sub>, P<sub>k</sub></b>	recursive least squares intermediate variable
<b>S</b>	covariance matrix
T3	high-pressure compressor outlet pressure
T6	low-pressure turbine exhaust temperature
<i>u</i>	input
wf	fuel flow
w <sub>k</sub>	weight coefficient
<b>W</b>	signal subspace
<b>x</b>	state variable
<b>y</b>	measurement/output
<b>z</b>	I/O stack vector
α, β, γ	forgetting factor
$\bar{\Gamma}_f$	generalized observable matrix
$\Phi_k$	Markov parameter vector
$\xi_k$	observation vector

### Abbreviations

Eig	eigenvalue
FF	forgetting factor
FHA	finite history recursive algorithm
I/O	input and output
IHA	infinite history recursive algorithm
PAST	projection approximation subspace tracking
SVD	singular value decomposition
VWPAST	variable weight projection approximation subspace tracking

### Superscripts

†	Moore-Penrose inverse
T	transpose of a matrix

### Notations

⊗	Kronecker product
(1:m,:)	line 1 to line m and all columns
norm	normalization
diag(v, p)	placing the elements of vector v on the p-th diagonal. p = 0 denotes the main diagonal, with p > 0 located above the main diagonal and p < 0 located below it

the idea of utilizing digital twin for future aircraft development [5], that the concept began to gain wider recognition [6]. NASA's definition expanded the concept to encompass highly integrated simulation models, characterized by multi-physical fields, multi-scale dimensions, and multi-probability. In recent years, the definition of digital twin technology has evolved further, reflecting its growing significance and application in various fields. Tao et al. [7,8] defined digital twin technology as a sophisticated technical tool that integrates multi-physics, multi-scale, and multidisciplinary attributes. This technology features real-time synchronization, mapping, and high fidelity, enabling seamless interaction and integration between the physical and information worlds. They proposed a five-dimensional model and outlined six application criteria, providing valuable guidance for the advancement of digital twin technology. Additionally, they highlighted that the most prevalent application of digital twin currently lies in the prognosis and health management of equipment. By utilizing real-time mapping through the twin model, potential equipment issues can be identified promptly, significantly enhancing model-based condition monitoring.

Before the introduction of digital twin technology, numerous studies focused on model-based methods for gas turbine condition monitoring. Some of these studies have laid the theoretical foundation for condition monitoring using digital twin. The models primarily encompass three main categories: (1) Performance model [9,10]. This model is grounded in the operational mechanisms of gas turbines, encompassing thermodynamics, rotor dynamics, combustion, and control theory. (2) Linear model [11]. Linearization occurs around the steady-state operation point of the gas turbine using the partial derivative method and fitting method [12]; (3) Data-driven model [13,14]. This model is constructed directly from the input and output data of gas turbines, utilizing machine learning techniques and various neural networks, which is a "black box" model.

To construct an accurate performance model, one must first acquire a thorough understanding of the component characteristics of target gas turbine [15,16]. These are typically delineated through characteristic diagrams supplied by the manufacturer, which principally chart the interplay among flow rate, efficiency, rotational speed, and pressure ratio for both the compressor and turbine of the gas turbines. Second, to implement condition monitoring of gas turbines using performance models, it is necessary to embed a set of health variables (0–1) for the efficiency and flow of components. Subsequently, these health variables are obtained by solving the balance equations of the gas turbine, as illustrated in Fig. 1:

The premise and key are to obtain the error between the performance model output and the gas turbine measurements. Numerical methods or optimization algorithms can be employed to minimize this error. This process ultimately yields health variables, which, when observed for changes, enable effective monitoring of the gas turbine condition. The variations of health variables offer a monitoring feature into the condition of the gas turbines. The primary benefit of this approach lies in its interpretability, enabling the identification of specific components within the gas turbine that are exhibiting signs of performance deterioration. Li et al. [17] established a thermodynamic model for gas turbines, incorporating health variables into performance variables (flow and efficiency) and resolving these factors using the Newton-Raphson algorithm, thus enabling diagnosis of typical gas path faults. Ying et al. [18] developed a highly precise performance model for a gas turbine, which incorporates the effects of the intake and exhaust systems. Experimental results demonstrate that this approach effectively estimates the degradation condition of a gas turbine. Yin et al. [19] integrated performance variables with exhaust electrostatic signal to assess the state of gas turbines. The primary drawback of this approach lies in the model nonlinearity, which includes volume inertia, rotational inertia, and thermal inertia. These nonlinearities necessitate iterative calculations by both the numerical method and optimization algorithm, leading to significant consumption of computational resources and often failing to meet real-time requirements. Furthermore, the extensive number of variables in gas turbines complicates the solution process, frequently causing it to converge to a local optimum rather than the global one, thereby compromising the accuracy of the results obtained.

Gas path analysis (GPA) is a technique for condition monitoring that employs a linear model of gas turbines. The core principle of this method involves establishing a linear correlation between measurements and performance variables at a specific steady-state operating point. If the relationship matrix linking the performance variables to the measurements is reversible, then changes in the unmeasured performance variable can be determined by observing changes in the measurements. The advantage of a linear model lies in its simplicity and ability to satisfy real-time requirements. Additionally, it can be effectively integrated with a Kalman filter for fault diagnosis in gas turbines and sensors [20,21]. Subsequently, the multi-model approach [22] emerged and continued to evolve.

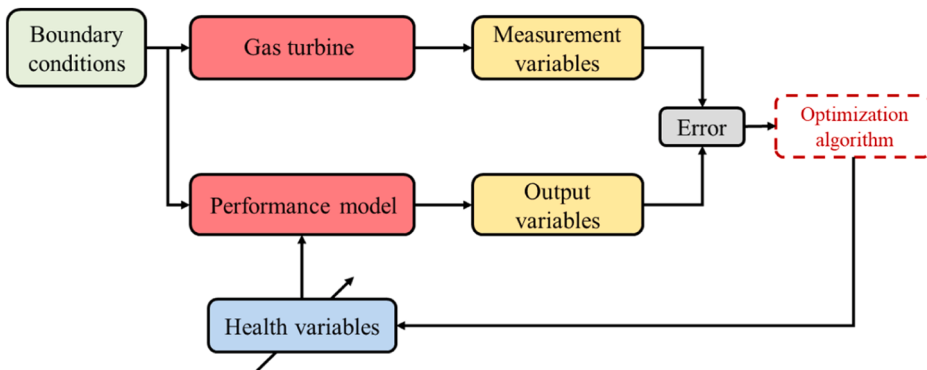


Fig. 1. Principle of condition monitoring based on performance model.

However, a primary limitation of the linear model is that it only functions effectively near specific steady-state operating points, which does not cater to the entire range of operating conditions in gas turbines. Consequently, numerous studies have introduced methods such as piecewise linearization [23] and linear time-varying models [24] to address this issue. Ma et al. [25] considered inlet guide vane angle as a scheduling parameter and proposed an enhanced two-layer variable parameter model. The study conducted in [26] utilized compressor speed as a scheduling parameter, employed polynomial fitting curve to design an linear parameter varying model, and established a dynamic adaptive model for turbofan engines. Even with improvements made to linear models, factors such as the selection of segment points and scheduling parameters continue to affect model accuracy.

With the advancement of computer technology, data-driven approaches are increasingly being applied to the modeling of gas turbines. By leveraging the abundant historical operational data of gas turbines, neural networks can effectively model the nonlinear components inherent in these systems. Utilizing techniques such as artificial neural networks (ANN) [27], extreme learning machines (ELM) [28], and nonlinear ARX (NARX) models [29], precise models of gas turbines can be established, which are then used for condition monitoring. In recent years, the application of deep learning methods, such as convolutional neural networks (CNN) [30] and long short-term memory (LSTM) [31], has been progressively expanding. These models possess distinct advantages in feature extraction, significantly advancing the field of condition monitoring technology. Cheng et al. [32] introduced a spatial-temporal graph neural network that incorporates prior physical knowledge, effectively leveraging the spatial coupling between knowledge and data. Zhang et al. [33] proposed a method combining Bidirectional Gated Recurrent Unit (BiGRU) and Multi-gate Mixture-of-Experts (MMoE) for simultaneous aero-engines condition assessment and remaining useful life prediction, enhancing the efficiency of health management tasks. Cheng et al. [34] constructed a component model of gas turbines, which they combined with ANN to create an surrogate model. They utilized the unscented Kalman filter to derive performance variables, facilitating diagnosis under both gradual degradation and sudden faults. The limitation of the data-driven modeling approach lies in its reliance on the quantity and quality of historical data. When the data set is limited, the model is susceptible to overfitting or underfitting. Although machine learning methods such as Bayesian model [35] and Gaussian regression [36] can be effective with limited data, they often face increased computational complexity when dealing with high-dimensional problems. Furthermore, relying solely on data-driven methods does not adequately account for the degradation of gas turbine performance.

The advent of digital twin technology has undeniably elevated the condition monitoring of gas turbines based on models to a new level [37]. Numerous scholars have explored the application of digital twin technology in gas turbine modeling for condition monitoring. They constructed the digital twin model using performance model, data-driven model, etc., or introduced a novel algorithm to address the associated challenges. Sun et al. [38] developed a gas turbine data-driven digital twin model using semi-supervised deep learning methods for performance monitoring and degradation prediction. This model was validated using real turbofan engines data and C-MAPSS dataset. The performance model and measurement data were integrated by Hu et al. [39] to enhance the simulation accuracy of the gas turbine, while introducing controlled errors into the model to reduce the modeling cycle. The gas turbine digital twin modeling method proposed by Zhang et al. [40] is based on deep multiple models, establishing a bidirectional data flow between the performance model and the data-driven model by integrating deep multiple models. Ma et al. [41] introduced a data-driven approach for developing a digital twin model of gas turbines, aiming to enhance anomaly detection capabilities in the field. Wang et al. [42] proposed a digital twin framework for aeroengine, aiming at engine fault diagnosis. Zhao et al. [43] utilized a reduced order model to establish a digital twin model of offshore wind turbines for modal analysis and corresponding structural prediction.

It can be seen from the above analysis that enhancing the precision of the model and the efficiency of the modeling process, along with establishing bidirectional communication between the model and its physical entity, stand as key objectives in the advancement of digital twin framework. As noted in the literature [44], surrogate modeling is an effective approach to accomplish the aforementioned tasks. The models discussed in the above literatures are referred to as surrogate models. Essentially, the surrogate model serves as a generalized digital twin model, typically integrated within the digital twin framework. Its primary function is to process the collected data and establish the mapping relationship between input and output data within the digital twin framework. In this process, it is essential to consider modeling accuracy, cost, and efficiency to fulfill the real-time requirements of digital twin.

One significant characteristic of the digital twin technology is that the output from the surrogate model consistently aligns with the measurements from the physical entity, regardless of whether the entity is normal or faulty. Under normal conditions, the structure of the surrogate model remain unchanged. However, when a fault occurs in the physical entity, the structure of the surrogate model must adapt since its output needs to match the altered measurements. Consequently, the usual correlation between input and output in the original surrogate model is disrupted. This adaptation becomes a critical attribute in condition monitoring, a fact supported by numerous studies highlighting the importance of changes in the model structure for condition monitoring.

Bartelmus et al. [45] established a linear correlation between operational conditions and spectral characteristics, utilizing the slope of the regression equation as a diagnostic feature to assess the planetary gearbox by monitoring changes in slope. Building upon this foundation, they further established a relationship between the root-mean-square value of the gear box's monitoring signal and load to enable fault detection under time-varying non-stationary loads [46]. The linear relationship between load power and vibration variables of wind turbine bearing was established in Zimroz et al. [47] based on this concept. The effectiveness of this approach was further validated through typical bearing failures. The problem of model mismatch in the actual process was revealed in Ceci et al. [48] through the analysis of structural equation models. The research conducted by Gui et al. [49] demonstrated that the demagnetization failure of a permanent magnet synchronous motor leads to discrepancies in model parameters and a decrease in model prediction accuracy.

Incorporating this concept into the digital twin framework allows for a form of "bidirectional communication" through the use of the surrogate model structural adjustments to relay condition information from the physical entity. This means the actual measurements from the physical entity can be used to update the surrogate model, while modifications in the surrogate model structure can be

employed to deduce information about the physical entity.

To address the constraints encountered by performance models, linear models, and data-driven models in the arena of gas turbine condition monitoring, this study establishes a gas turbine surrogate model for condition monitoring and explores the application of surrogate model in the development of gas turbine digital twin. The surrogate model employs a linear framework to maintain computational efficiency. It does not require extensive historical operational data and remains effective across the entire operating range of the gas turbine. In addition, in our review of the literature on gas turbine modeling, we have discovered that a limited number of studies address the issue of closed-loop control. Specifically, the interplay between system input and noise often results in skewed estimations from the model, which is also one of the issues that needs to be addressed. The premise and key to obtain the model parameters online is to be able to obtain the generalized observable matrix of the linear model online. To address above issues, this study introduces a method based on Markov-projection approximation subspace tracking (Markov-PAST). PAST method in array signal processing is an effective approach to computing and updating the subspace of a matrix. The challenging task lies in finding an appropriate observation vector. The observation vector contains the information of the signal subspace, so in this study, a Markov parameter matrix is constructed to derive this observation vector. Utilizing the PAST method, the signal subspace of the observed vector autocorrelation matrix is computed. This computation transforms the calculation of the signal subspace into an unconstrained optimization problem, which is then obtained through recursive calculation. The impact of closed-loop interference is mitigated by minimizing noise. Subsequently, the signal subspace in the recursive process is equivalent to the generalized observable matrix, and the model parameters are extracted from the generalized observable matrix. The model is continually updated in real-time using data gathered by sensors, ensuring that the outputs align closely with the actual the gas turbine.

The primary contributions of this research are outlined as follows: (1) A gas turbine surrogate model for condition monitoring is established, which is applicable in the development of the gas turbine digital twin. (2) The surrogate model is updated in real-time using the Markov-PAST method. (3) A refined form of the PAST method has been proposed to enhance the algorithm robustness in the presence of impulsive noise. (4) The modeling process takes into account the impact of the closed-loop system. (5) The effectiveness of the surrogate model for condition monitoring is corroborated through both simulation data and experiment data.

This study is outlined as follows: [Section 2](#) is an introduction to the research object. [Section 3](#) introduces the relevant methodology. [Section 4](#) details the entire modeling process. [Section 5](#) presents the verification results of the model, and [Section 6](#) concludes with the main findings and future prospects.

## 2. Principle of gas turbine

In this study, we have selected a propulsion-type three-shaft gas turbine as the research objective. This gas turbine boasts a rated power output of 26.2 MW, making it ideal for the power systems of large vessels. [Fig. 2](#) is the schematic diagram of the three-shaft gas turbine, and [Table 1](#) is the primary design parameters and variables.

The three-shaft gas turbine consists of low-pressure compressor, high-pressure compressor, combustion chamber, high-pressure turbine, low-pressure turbine, and power turbine. The operational process is as follows: Initially, during startup, the motor drives the compressor to rotate. Air enters the compressor through the inlet filter where impurities such as large dust particles are filtered out. The compressed air then flows into the combustion chamber where its pressure and temperature increase. Fuel is injected into the combustion chamber and ignition occurs after mixing with high temperature and high pressure gas. Intense combustion generates gas with even higher temperature and pressure in the combustion chamber. Subsequently, this gas sequentially enters each turbine stage driving their rotation the high-pressure turbine drives the high-pressure compressor while the low-pressure turbine drives the low-pressure compressor. Once started up successfully, disconnection from starter allows for stable operation of the gas turbine; meanwhile, power generated by the power turbine performs work on loads. It should be noted that during operation of a gas turbine system, cavities ( $V_1, V_2, V_3$ ) between components cannot be disregarded; airflow passing through these areas adheres to mass conservation principles. Additionally worth mentioning is that due to its significant mass and rotational inertia characteristics, the rotating shaft of a gas turbine complies with dynamic equations. In [Fig. 2](#), 0 represents the atmospheric environment, 1 represents the inlet section of the

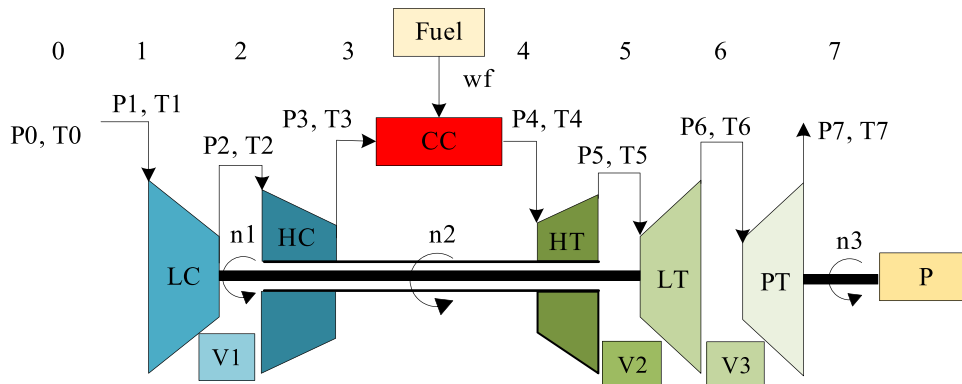


**Fig. 2.** Schematic diagram of three-shaft gas turbine structure.

**Table 1**

Main variables/ parameters of three-shaft gas turbine.

Variables/ Parameters	Unit	Value (Type)
Low-pressure rotor speed ( $n_1$ )	r/min	7168
High-pressure rotor speed ( $n_2$ )	r/min	9564
Power turbine speed ( $n_3$ )	r/min	3260
outlet temperature of the low-pressure compressor (T2)	K	465
outlet temperature of the high-pressure compressor (T3)	K	739
outlet temperature of the low-pressure turbine (T6)	K	1004
outlet pressure of the low-pressure compressor (P2)	kPa	438
outlet pressure of the high-pressure compressor (P3)	kPa	1978
outlet pressure of the low-pressure turbine (P6)	kPa	358
Rating power ( $P$ )	MW	26.2
Efficiency	%	36.3
Fuel	—	Diesel oil

low-pressure compressor, 2 represents the inlet section of the high-pressure compressor, 3 represents the inlet section of the combustion chamber, 4 represents the inlet section of the high-pressure turbine, 5 represents the inlet section of the low-pressure turbine, 6 represents the inlet section of the power turbine, and 7 represents the outlet section of the power turbine.

As depicted in Fig. 3, the three-shaft gas turbine employs a closed-loop control strategy to regulate the power turbine speed. Upon receiving the power command signal  $P$ , the control system automatically calculates the current speed  $n_{3,0}$  of the power turbine and determines the difference  $\Delta n_3$  between its actual speed  $n_3$  and given speed  $n_{3,0}$  as input for a controller that typically utilizes PID control methodology. The PID controller is designed based on predetermined  $K_p$ ,  $K_b$ ,  $K_d$  values, which are then used to calculate the required fuel flow  $wf$  for energy conversion into kinetic energy reflected in rotor rotation. A sensor measures power turbine speed and feeds it back into the controller forming a closed-loop, thereby enabling maintenance of set working condition.

### 3. Methodology

#### 3.1. Surrogate modeling principle

The surrogate model developed in this research is based on the linear model framework, utilizing the state-space model from modern control theory, which is widely applied in practical engineering. As discussed in the introduction, the benefits of the linear model include its simple structure and low computational requirements, ensuring efficient online calculations. Linear models are somewhat limited, effectively applicable only in the vicinity of a specified steady-state operating point. To overcome this limitation, various adaptations, such as piecewise linear models and linear time-varying models, have been introduced. Despite these enhancements, challenges remain with selecting appropriate segment points and scheduling parameters, which affects the model accuracy. Consequently, the model outputs often fail to track the actual measurements of gas turbine in real-time and accurately. To address this issue, the study introduces the principle of surrogate modeling, which is shown in Fig. 4:

The input and measurements are collected in real-time from a real gas turbine, and the model parameters are derived through identification techniques. At  $k=1$ , the surrogate model receives the input  $u_1$  and measurements  $y_1$ , resulting in the identification results  $A_1$ ,  $B_1$ ,  $C_1$ ,  $K_1$ . Subsequently, at  $k=2$ , the model receives the input  $u_2$  and measurements  $y_2$ , yielding the identification results  $A_2$ ,  $B_2$ ,  $C_2$ ,  $K_2$ . This process continues iteratively for subsequent time. The outputs of the model at time  $k$  are derived from the model parameters  $A_{k,p}$ ,  $B_{k,p}$ ,  $C_{k,p}$ ,  $K_{k,p}$ , which are established prior to time  $k$ , as well as from the input and measurements. This approach considers the dynamic behavior of the gas turbine, with the particular computational method to be detailed subsequently. The established model can be considered a linear time-varying model, where its parameters evolve over time. However, unlike traditional time-varying models, this surrogate model does not require the determination of scheduling parameters. This eliminates the error typically introduced when establishing the relationship between scheduling parameters and the model output characteristics. The core of the established surrogate model lies in solving its parameters at each moment, ensuring that the process is not overly complex to maintain accuracy and efficiency, which is a key focus of this study. Furthermore, as the surrogate model must address the closed-loop issue, it is essential to eliminate the influence of  $e_k$  within the algorithm.

Online acquisition of model parameters can be achieved through two methods: the finite history recursive algorithm (FHA) and the infinite history recursive algorithm (IHA), also known as sliding window algorithm and exponential window algorithm [50], as depicted in Fig. 5.

FHA involves conducting an identification process within a limited window each time new data is collected, integrating it with

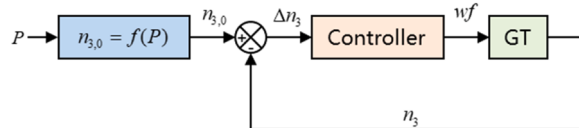


Fig. 3. Closed-loop control strategy for three-shaft gas turbines.

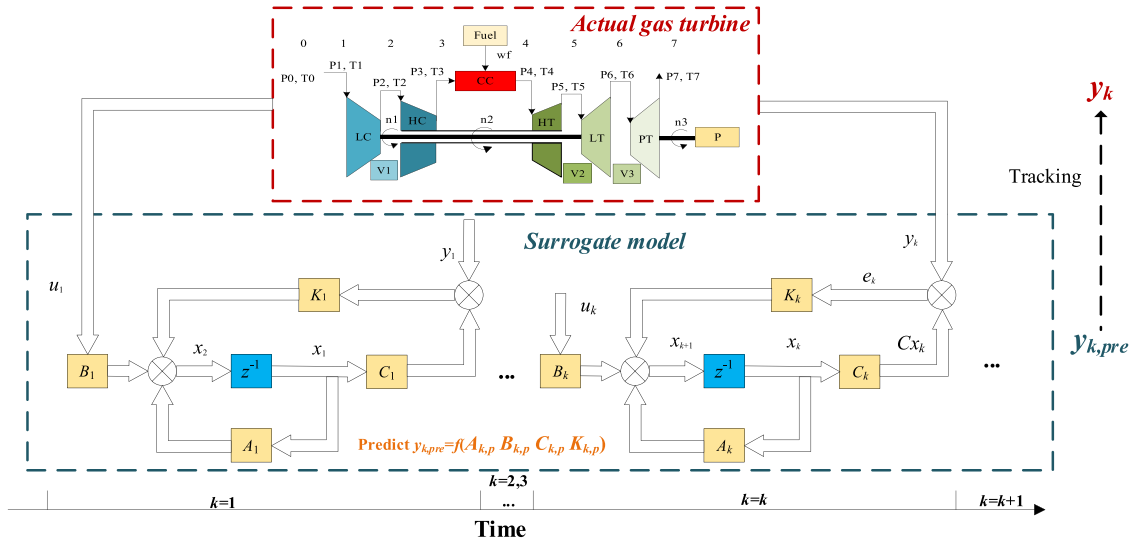


Fig. 4. Gas turbine surrogate modeling principle.

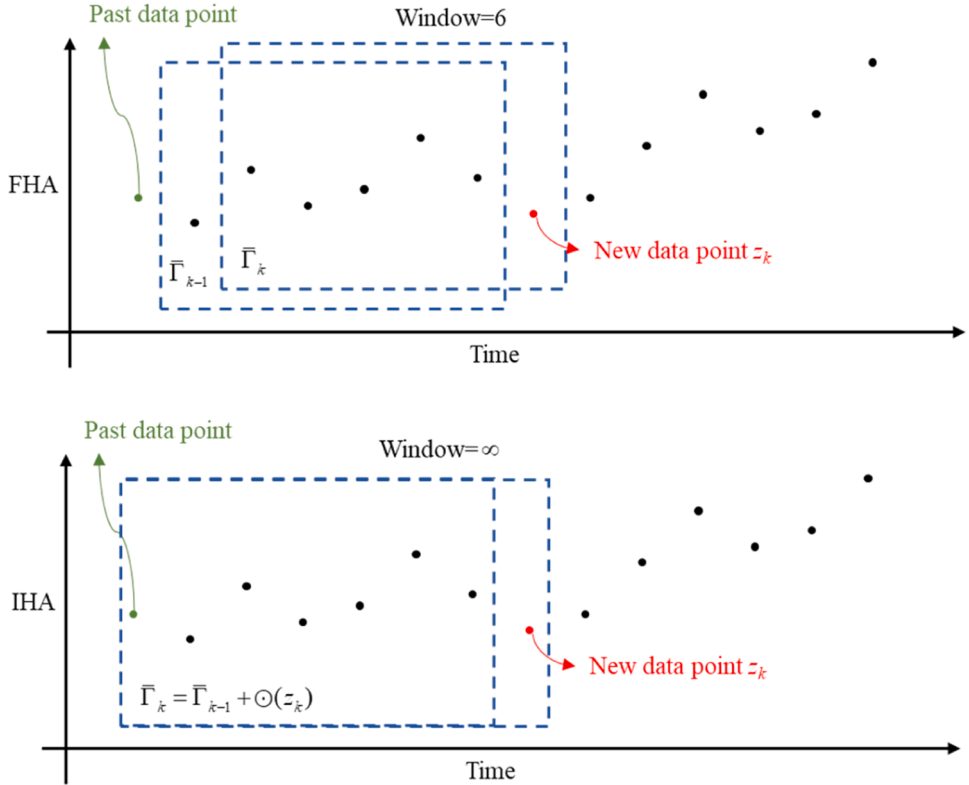


Fig. 5. Principles of FHA and IHA.

historical operating data. The key to obtain the model parameters is to calculate the generalized observable matrix. This approach enables the effective utilization of the most recent data to update a generalized observable matrix, facilitating the identification of the current model. Importantly, as the system transitions to a new state, past data does not influence the characteristics of the current model. One drawback is that window size must be carefully calibrated. Each identification procedure entails SVD and the projection method is used to eliminate noise. If this process is carried out in a large window, the efficiency of the calculation will be reduced. Conversely, a window that is too small might fail to accurately capture the system dynamic properties. To obtain generalized observable matrix online using the FHA, performing SVD in each window is feasible. While executing SVD with a computer is not

inherently complex, doing so within each window consistently requires a significant amount of computing resources. Most significantly, since a gas turbine exemplifies a closed-loop system, a correlation exists between the noise and the input. Consequently, employing projection to negate noise impact is not a feasible approach. However, IHA does not need to consider window size. This method only needs to initialize generalized observable matrix once and then use the latest data collected to update it. This method greatly reduces computing resources and does not need to store the data in the window, which is especially suitable for online processes. One drawback is the requirement to utilize the entirety of past data, which can lead to error accumulation. Consequently, in practical computations, it is common to apply a forgetting factor, typically close to 1, to mitigate the influence of historical information.

In this study, IHA is adopted for online calculation, and a Markov-PAST method is proposed. The subspace tracking approach within array signal processing serves as an effective method to dynamically update the matrix subspace. The challenge and key of applying this method to solve for the generalized observable matrix lie in identifying an appropriate observation vector that encapsulates the essential information of generalized observable matrix. In this paper, a method is proposed to derive the observation vector by constructing a Markov parameter matrix. The PAST method is then employed to compute and update the signal subspace of the observation vector autocorrelation matrix. The signal subspace is treated as equivalent to generalized observable matrix. Subsequently, the calculation for generalized observable matrix is transformed into an unconstrained optimization problem, which is obtained through recursive calculations. Finally, model parameters are derived from generalized observable matrix to obtain the structure of the online surrogate model. During this phase, the recursive least square method is applied to minimize noise and mitigate the impact of closed-loop identification.

Generally, the process of establishing the surrogate model relies on the Markov-PAST. The model is continuously updated with the last data collected at each moment, ensuring that the model output accurately tracks the actual measurements in real time.

### 3.2. Markov-PAST method

This section introduces the Markov-PAST method to the establishment of the surrogate model. Firstly, the state-space model [51] of the gas turbine is written as modified form, as shown in Eq. (1):

$$\begin{cases} \hat{\mathbf{x}}_{k+1} = \mathbf{A}\hat{\mathbf{x}}_k + \mathbf{B}\mathbf{u}_k + \mathbf{K}\mathbf{e}_k, \\ \hat{\mathbf{y}}_k = \mathbf{C}\hat{\mathbf{x}}_k + \mathbf{e}_k \end{cases} \quad (1)$$

where the variables  $\mathbf{u} = [u_1 \ u_2 \ \dots \ u_j]^T \in \mathbb{R}^j$ ,  $\hat{\mathbf{y}} = [y_1 \ y_2 \ \dots \ y_m]^T \in \mathbb{R}^m$ ,  $\hat{\mathbf{x}} = [x_1 \ x_2 \ \dots \ x_n]^T \in \mathbb{R}^n$  represent the input, model output, and model state variables respectively. The measurements of gas turbine involve directly measuring variables such as temperature, speed, and pressure in the cross-section of the gas turbine. The input typically consists of the gas turbine fuel flow.

$$\mathbf{A} = \begin{bmatrix} a_{11} & a_{12} & \dots & a_{1n} \\ a_{21} & a_{22} & \dots & a_{2n} \\ \vdots & \vdots & \ddots & \vdots \\ a_{n1} & a_{n2} & \dots & a_{nn} \end{bmatrix} \in \mathbb{R}^{n \times n}, \mathbf{B} = \begin{bmatrix} b_{11} & b_{12} & \dots & b_{1j} \\ b_{21} & b_{22} & \dots & b_{2j} \\ \vdots & \vdots & \ddots & \vdots \\ b_{n1} & b_{n2} & \dots & b_{nj} \end{bmatrix} \in \mathbb{R}^{n \times j}, \mathbf{C} = \begin{bmatrix} c_{11} & c_{12} & \dots & c_{1n} \\ c_{21} & c_{22} & \dots & c_{2n} \\ \vdots & \vdots & \ddots & \vdots \\ c_{m1} & c_{m2} & \dots & c_{mn} \end{bmatrix} \in \mathbb{R}^{m \times n}$$

represent the parameter matrices.  $\mathbf{K} = \begin{bmatrix} k_{11} & k_{12} & \dots & k_{1m} \\ k_{21} & k_{22} & \dots & k_{2m} \\ \vdots & \vdots & \ddots & \vdots \\ k_{n1} & k_{n2} & \dots & k_{nm} \end{bmatrix} \in \mathbb{R}^{n \times m}$  denotes the Kalman filter gain, while  $\mathbf{e}_k = \mathbf{y}_k - \mathbf{C}\hat{\mathbf{x}}_k$  signifies the mean white noise process.

The primary objective of this study is to ascertain the parameter matrix by utilizing gas turbine input and measurement data. Consequently, both the output and state variables of the model are denoted as  $\mathbf{y}_k$  and  $\mathbf{x}_k$  in subsequent discussions.

The state-space model should be transformed into the predictor form as follows [52]:

$$\begin{cases} \mathbf{x}_{k+1} = \bar{\mathbf{A}}\mathbf{x}_k + \bar{\mathbf{B}}\mathbf{z}_k, \\ \mathbf{y}_k = \mathbf{C}\mathbf{x}_k + \mathbf{e}_k \end{cases} \quad (2)$$

where  $\mathbf{z} = [\mathbf{u}^T \ \mathbf{y}^T]^T \in \mathbb{R}^{m+j}$ ,  $\bar{\mathbf{A}} = \mathbf{A} - \mathbf{K}\mathbf{C} \in \mathbb{R}^{n \times n}$

$$\bar{\mathbf{B}} = [\mathbf{B} \ \ \mathbf{K}] = \begin{bmatrix} b_{11} & b_{12} & \dots & b_{1j} & k_{11} & k_{12} & \dots & k_{1m} \\ b_{21} & b_{22} & \dots & b_{2j} & k_{21} & k_{22} & \dots & k_{2m} \\ \vdots & \vdots & \ddots & \vdots & \vdots & \vdots & \ddots & \vdots \\ b_{n1} & b_{n2} & \dots & b_{nj} & k_{n1} & k_{n2} & \dots & k_{nm} \end{bmatrix} \in \mathbb{R}^{n \times (m+j)}.$$

**Assumption 1.**  $\|\bar{\mathbf{A}}\| \leq 1$ .

In Assumption (1), the eigenvalues of matrix  $\bar{\mathbf{A}}$  are situated within the unit circle. The foundational premise of this study is the stability of the system. As noted in reference [53], the discrete system exhibits asymptotic stability when the eigenvalues of the state-space model system fall within the unit circle.

The forward recurrence allows us to derive the following:

$$\mathbf{y}_{f,k} = \bar{\mathbf{F}}_f \mathbf{x}_k + \bar{\mathbf{H}}_f \mathbf{z}_{f-1,k} + \mathbf{e}_{f,k}, \quad (3)$$

where

$$\mathbf{y}_{f,k} = \left[ \mathbf{y}_k^T \mathbf{y}_{k+1}^T \cdots \mathbf{y}_{k+f-1}^T \right]^T \in \mathbb{R}^{mf},$$

$$\mathbf{z}_{f-1,k} = \left[ \mathbf{z}_k^T \mathbf{z}_{k+1}^T \cdots \mathbf{z}_{k+f-2}^T \right]^T \in \mathbb{R}^{(m+j)(f-1)},$$

$$\mathbf{e}_{f,k} = \left[ \mathbf{e}_k^T \mathbf{e}_{k+1}^T \cdots \mathbf{e}_{k+f-1}^T \right]^T \in \mathbb{R}^{mf},$$

$$\bar{\Gamma}_f = \begin{bmatrix} \mathbf{C} \\ \mathbf{CA} \\ \vdots \\ \mathbf{CA}^{f-1} \end{bmatrix} \in \mathbb{R}^{mf \times n},$$

$$\bar{\mathbf{H}}_f = \begin{bmatrix} \mathbf{0} & \mathbf{0} & \cdots & \mathbf{0} \\ \mathbf{CB} & \mathbf{0} & \cdots & \mathbf{0} \\ \mathbf{CAB} & \mathbf{CB} & \cdots & \mathbf{0} \\ \vdots & \vdots & \ddots & \mathbf{0} \\ \mathbf{CA}^{f-2}\mathbf{B} & \mathbf{CA}^{f-3}\mathbf{B} & \cdots & \mathbf{CB} \end{bmatrix} \in \mathbb{R}^{mf \times (m+j)(f-1)}.$$

The Eq. (3) is expressed in the form of a Hankel matrix as shown below:

$$\mathbf{Y}_f = \bar{\Gamma}_f \mathbf{X}_k + \bar{\mathbf{H}}_f \mathbf{Z}_{f-1} + \mathbf{E}_f, \quad (4)$$

where

$$\mathbf{X}_k = [\mathbf{x}_k \mathbf{x}_{k+1} \cdots \mathbf{x}_{k+R-1}] \in \mathbb{R}^{n \times R},$$

$$\mathbf{Y}_f = [\mathbf{y}_{f,k} \mathbf{y}_{f,k+1} \cdots \mathbf{y}_{f,k+R-1}] \in \mathbb{R}^{mf \times R},$$

$$\mathbf{Z}_{f-1} = [\mathbf{z}_{f-1,k} \mathbf{z}_{f-1,k+1} \cdots \mathbf{z}_{f-1,k+R-1}] \in \mathbb{R}^{(m+j)(f-1) \times R},$$

$$\mathbf{E}_f = [\mathbf{e}_{f,k} \mathbf{e}_{f,k+1} \cdots \mathbf{e}_{f,k+R-1}] \in \mathbb{R}^{mf \times R},$$

where  $R$  represents the number of columns in the Hankel matrix.

**Assumption 2.**  $\text{rank}(\mathbf{Z}_{f-1}) = R$ .

In Assumption (2), the model parameters obtained by the identification method will converge to the true parameters when the input signal satisfies the persistency of excitation [54,55]. In addition, the model should aim to adhere to the principle of minimum implementation to ensure it has the smallest order and highest computational efficiency while maintaining accuracy. Although this condition is not a necessary prerequisite, it is the objective of the optimization model.

In open-loop identification, where noise is uncorrelated with input and output, projection methods are often employed to mitigate the impact of noise. For instance, oblique projection techniques are widely referenced in literature [56,57], with the N4SID method being an exemplary case of offline subspace identification. More broadly, on both sides of the equation, the row space is projected onto the row space of the complement of  $\mathbf{Z}_{f-1}$ , resulting in the following equation:

$$\mathbf{Y}_f \Pi_{\mathbf{Z}_{f-1}}^\perp = \bar{\Gamma}_f \mathbf{X}_k \Pi_{\mathbf{Z}_{f-1}}^\perp + \bar{\mathbf{H}}_f \mathbf{Z}_{f-1} \Pi_{\mathbf{Z}_{f-1}}^\perp + \mathbf{E}_f \Pi_{\mathbf{Z}_{f-1}}^\perp, \quad (5)$$

According to the properties of the projection, the following equation is obtained:

$$\mathbf{Y}_f \Pi_{\mathbf{Z}_{f-1}}^\perp = \bar{\Gamma}_f \mathbf{X}_k \Pi_{\mathbf{Z}_{f-1}}^\perp + \mathbf{E}_f, \quad (6)$$

A standard approach involves multiplying by two factors  $\mathbf{O}_1, \mathbf{O}_2$ , which must satisfy the following conditions:

$$\text{rank}(\mathbf{O}_1 \bar{\Gamma}_f) = \text{rank}(\bar{\Gamma}_f)$$

$$\text{rank}(\mathbf{X}_k \Pi_{\mathbf{Z}_{f-1}}^\perp \mathbf{O}_2) = \text{rank}(\mathbf{X}_k),$$

$$\mathbf{O}_1 \mathbf{E}_f \mathbf{O}_2 = \mathbf{O}$$

Depending on the method of identification used, the factors  $\mathbf{O}_1, \mathbf{O}_2$  will vary. For detailed procedures, one should consult the referenced literature [58]. Subsequently, SVD is performed to obtain the generalized observability matrix  $\bar{\Gamma}_f$ .

However, the presence of the closed-loop invalidates the condition that the noise is unrelated to the input/output, thereby rendering the aforementioned process unfeasible. Therefore, based on the form of IHA, this study adopts the following process to obtain the generalized observable matrix:

The backward recursion of Eq. (2) over  $p$  time domains yields:

$$\mathbf{x}_k = \bar{\mathbf{A}}^p \mathbf{x}_{k-p} + \sum_{i=1}^p \bar{\mathbf{A}}^{i-1} \bar{\mathbf{B}} \mathbf{z}_{k-i}, \quad (7)$$

The Assumption (1) implies that  $\|\bar{\mathbf{A}}\| \leq 1$ . Therefore, if  $p$  exceeds a certain threshold, we can conclude that  $\bar{\mathbf{A}}^p \mathbf{x}_{k-p} \approx 0$  and consequently obtain:

$$\mathbf{x}_k = \sum_{i=1}^p \bar{\mathbf{A}}^{i-1} \bar{\mathbf{B}} \mathbf{z}_{k-i}, \quad (8)$$

The truncation of Eq. (8) at  $p$  yields the following result:

$$\mathbf{x}_k = [\bar{\mathbf{A}}^{p-1} \bar{\mathbf{B}} \bar{\mathbf{A}}^{p-2} \bar{\mathbf{B}} \dots \bar{\mathbf{B}}] \begin{bmatrix} \mathbf{z}_{k-p}^T \\ \mathbf{z}_{k-p+1}^T \\ \vdots \\ \mathbf{z}_{k-1}^T \end{bmatrix} = \mathbf{L}_p \mathbf{Z}_{p,k}, \quad (9)$$

The Eq. (9) can be derived by expressing it in the form of a Hankel matrix:

$$\mathbf{X}_k = \mathbf{L}_p \mathbf{Z}_p, \quad (10)$$

where  $\mathbf{Z}_p = [\mathbf{z}_{p,k} \ \mathbf{z}_{p,k-1} \ \dots \ \mathbf{z}_{p,k+R-1}] \in \mathbb{R}^{(m+j)p \times R}$ .

The Markov parameter matrix is defined as follows:

$$\mathbf{M} = \bar{\Gamma}_f \mathbf{L}_p = \begin{bmatrix} \mathbf{C} \\ \bar{\mathbf{C}} \bar{\mathbf{A}} \\ \vdots \\ \bar{\mathbf{C}} \bar{\mathbf{A}}^{f-1} \end{bmatrix} [\bar{\mathbf{A}}^{p-1} \bar{\mathbf{B}} \ \bar{\mathbf{A}}^{p-2} \bar{\mathbf{B}} \ \dots \ \bar{\mathbf{B}}], \quad (11)$$

where  $\mathbf{M} \in \mathbb{R}^{mf \times (m+j)p}$ .

If  $\mathbf{h}_i = \bar{\mathbf{C}} \bar{\mathbf{A}}^{i-1} \bar{\mathbf{B}}$ ,

$$\mathbf{M} = \begin{bmatrix} \mathbf{h}_p & \mathbf{h}_{p-1} & \dots & \mathbf{h}_1 \\ \mathbf{h}_{p+1} & \mathbf{h}_p & \dots & \mathbf{h}_2 \\ \vdots & \vdots & \ddots & \vdots \\ \mathbf{h}_{p+f-1} & \mathbf{h}_{p+f-2} & \dots & \mathbf{h}_f \end{bmatrix}, \quad (12)$$

When  $p$  is large enough,

$$\mathbf{M} = \begin{bmatrix} \mathbf{h}_p & \mathbf{h}_{p-1} & \dots & \mathbf{h}_1 \\ 0 & \mathbf{h}_p & \dots & \mathbf{h}_2 \\ \vdots & \vdots & \ddots & \vdots \\ 0 & 0 & \dots & \mathbf{h}_f \end{bmatrix}, \quad (13)$$

The Eq. (8) is incorporated into Eq. (1), resulting in the following derived equation:

$$\mathbf{y}_k = \sum_{i=1}^p \bar{\mathbf{C}} \bar{\mathbf{A}}^{i-1} \bar{\mathbf{B}} \mathbf{z}_{k-i} + \mathbf{e}_k = \sum_{i=1}^p \mathbf{h}_i \mathbf{z}_{k-i} + \mathbf{e}_k, \quad (14)$$

The given equation represents an ARX model of order  $p$ , which is also the method used to calculate the output of the surrogate model, where the coefficient  $\mathbf{h}$  denotes the Markov parameter of the predictor.

The Eq. (14) should be reformulated as:

$$\mathbf{y}_k = \boldsymbol{\varphi} \mathbf{z}_{p,k} + \mathbf{e}_k, \quad (15)$$

where  $\boldsymbol{\varphi} = [\bar{\mathbf{C}} \bar{\mathbf{B}} \ \bar{\mathbf{C}} \bar{\mathbf{A}} \bar{\mathbf{B}} \ \dots \ \bar{\mathbf{C}} \bar{\mathbf{A}}^{p-1} \bar{\mathbf{B}}] \in \mathbb{R}^{m \times (m+j)p}$  is called Markov parameter vector.

The problem thus transforms into an optimization problem with given  $\mathbf{z}_{p,k}$  and  $\mathbf{y}_k$ , specifically aiming to minimize the following criteria, which is an approach to mitigate the impact of noise:

$$J(\boldsymbol{\varphi}) = \mathbf{e}_k = \sum_{k=1}^L \| \mathbf{y}_k - \boldsymbol{\varphi} \mathbf{z}_{p,k} \|^2, \quad (16)$$

The recursive least squares method presented below is employed for  $\boldsymbol{\varphi}$ :

$$\begin{aligned}\varphi_k &= \varphi_{k-1} + (\mathbf{y}_k - \varphi_{k-1} \mathbf{z}_{p,k}) \mathbf{Q}_k \\ \mathbf{Q}_k &= \frac{\mathbf{z}_{p,k}^T \mathbf{P}_{k-1}}{\beta + \mathbf{z}_{p,k}^T \mathbf{P}_{k-1} \mathbf{z}_{p,k}}, \\ \mathbf{P}_k &= \frac{(\mathbf{P}_{k-1} - \mathbf{P}_{k-1} \mathbf{z}_{p,k} \mathbf{Q}_k)}{\beta}\end{aligned}\quad (17)$$

$$\mathbf{P}_k^{-1} = \mathbf{z}_{p,k} \mathbf{z}_{p,k}^T \in \mathbb{R}^{(m+j)p \times (m+j)p}, \varphi = \mathbf{E}_{yz} (\mathbf{E}_{zz})^{-1}, \mathbf{E}_{yz} = \sum_{i=1}^R \mathbf{y}_k \mathbf{z}_{p,k}^T \in \mathbb{R}^{m \times (m+j)p},$$

where

$$\mathbf{E}_{zz} = \sum_{i=1}^R \mathbf{z}_{p,k} \mathbf{z}_{p,k}^T \in \mathbb{R}^{(m+j)p \times (m+j)p}, \beta$$

this is to "discard" past information during recursion, in order to prevent the past data from overwhelming the new data and causing the algorithm to lose its ability to adjust parameters, meanwhile, avoid the accumulation of errors. The other forgetting factors in this study have equivalent effects and will not be further discussed. The selection of the forgetting factor significantly influences both the convergence speed of the algorithm and the accuracy of the model [59,60].

The major advantage of the PAST lies in its ability to circumvent SVD during the identification process and instead transforms the estimation of the generalized observable matrix into an unconstrained optimization problem [61]. The problem can be formulated as follows: Consider the observation vector  $\xi$  and the criterion function below, where  $\mathbf{W}$  represents the signal subspace of autocorrelation matrix of observation vector:

$$J(\mathbf{W}) = E \left\{ \| \xi - \mathbf{W} \mathbf{W}^T \xi \|^2 \right\}, \quad (18)$$

The criterion function is reformulated into a recursive form incorporating a forgetting factor,  $0.9 \leq \alpha \leq 1$ :

$$J(\mathbf{W}_k) = \sum_{t=1}^k \alpha^{k-t} \| \xi_t - \mathbf{W}_k \mathbf{W}_k^T \xi_t \|^2, \quad (19)$$

If  $\mathbf{d}_t = \mathbf{W}_k^T \xi_t$ , Eq. (19) can be written:

$$J(\mathbf{W}_k) = \sum_{t=1}^k \alpha^{k-t} \| \xi_t - \mathbf{W}_k \mathbf{d}_t \|^2, \quad (20)$$

The fundamental recurrence equations of the PAST are as follows:

$$\begin{aligned}\mathbf{d}_t &= \mathbf{W}_{t-1}^T \xi_t \\ \mathbf{g}_t &= \mathbf{K}_{t-1} \mathbf{d}_t \\ \mathbf{q}_t &= \mathbf{g}_t / (\alpha + \mathbf{d}_t^T \mathbf{g}_t) \\ \mathbf{K}_t &= [\mathbf{K}_{t-1} - \mathbf{q}_t \mathbf{g}_t^T] / \alpha, \\ \mathbf{e}_t &= \xi_t - \mathbf{W}_{t-1} \mathbf{d}_t \\ \mathbf{W}_t &= \mathbf{W}_{t-1} + \mathbf{e}_t \mathbf{q}_t^T\end{aligned}\quad (21)$$

The most crucial step among them is to employ the concept of approximate projection, wherein  $\mathbf{W}_{t-1}^T \xi_t$  replaces  $\mathbf{W}_t^T \xi_t$  for recursive purposes.  $\mathbf{g}_t, \mathbf{q}_t$  and  $\mathbf{e}_t$  serve as the intermediary variable in recursive calculations, while  $\alpha$  represents the forgetting factor.

The orthogonality of  $\mathbf{W}_k$  cannot be guaranteed by using  $\mathbf{W}_{t-1}^T \xi_t$  to replace  $\mathbf{W}_t^T \xi_t$  for recursion. Therefore, it is necessary to orthogonalize  $\mathbf{W}_k$  in each iteration during the calculation process, as demonstrated in Eq. (22):

$$\mathbf{W}_k = \mathbf{W}_k (\mathbf{W}_k^T \mathbf{W}_k)^{-1/2} \quad (22)$$

The Eq. (22) is expressed as a recursive relation in the following format:

$$\begin{aligned}\sigma_t &= \| \mathbf{q}_t \|^2 \left( (1 + \| \mathbf{e}_t \|^2 \| \mathbf{q}_t \|^2)^{-1/2} - 1 \right) \\ \mathbf{e}'_t &= \sigma_t \mathbf{W}_{t-1} \mathbf{q}_t + (1 + \| \mathbf{q}_t \|^2) \mathbf{e}_t \\ \mathbf{W}_t &= \mathbf{W}_{t-1} + \mathbf{e}'_t \mathbf{q}_t^T\end{aligned}\quad (23)$$

The challenge with PAST lies in identifying a suitable observation vector that incorporates information of the generalized observable matrix. In this study, we address this issue by employing a constructed Markov matrix to determine the observation vector, which can be derived from Eqs. (4), (8), and (11):

$$\bar{\Gamma}_f \mathbf{x}_k = \mathbf{M} \mathbf{z}_{p,k}, \quad (24)$$

The above equation implies that the column space of matrix  $\mathbf{M} \mathbf{z}_{p,k}$  is equivalent to the column space of matrix  $\bar{\Gamma}_{f,k}$ . Assuming  $\xi_k = \mathbf{M} \mathbf{z}_{p,k}$ , we can deduce that  $\mathbf{W}_k = \bar{\Gamma}_{f,k}$ . The initialization of  $\mathbf{W}_k$  allows for the selection of any matrix, however, in order to expedite

convergence of the PAST, it is recommended to obtain input and measurements from a length collected at the initial stage of the algorithm based on offline subspace identification [62].

The matrices  $\mathbf{A}$ ,  $\mathbf{B}$ ,  $\mathbf{C}$ , and  $\mathbf{K}$  can be obtained using  $\bar{\Gamma}_f$ :

$$\mathbf{C} = \bar{\Gamma}_{f,k}(1 : m, :), \quad (25)$$

where,  $m$  represents the dimension of output.

The last column of the Markov parameter matrix  $\mathbf{M}$  is acquired:

$$\mathbf{E} = \begin{bmatrix} \mathbf{CB} \\ \mathbf{CAB} \\ \vdots \\ \mathbf{CA}^{j-1}\mathbf{B} \end{bmatrix} = \bar{\Gamma}_{f,k}\bar{\mathbf{B}}, \quad (26)$$

Therefore

$$\begin{aligned} \bar{\mathbf{B}} &= \bar{\Gamma}_{f,k}^\dagger \mathbf{E} \\ \mathbf{B} &= \bar{\mathbf{B}}(:, 1:j), \\ \mathbf{K} &= \bar{\mathbf{B}}(:, j+1:j+m) \end{aligned}, \quad (27)$$

where the variable  $j$  represents the dimensionality of the input.

The shift invariant property of  $\bar{\Gamma}_f$  is utilized to obtain this:

$$\begin{aligned} \bar{\mathbf{A}} &= \bar{\Gamma}_{f,k}^\dagger(1 : n(f-1), :) \bar{\Gamma}_{f,k}(n+1 : nf, :), \\ \mathbf{A} &= \bar{\mathbf{A}} + \mathbf{KC} \end{aligned}, \quad (28)$$

where the dimension of the state variable is represented by  $n$ .

### 3.3. VWPAST method

The data received by the gas turbine from the sensor in practical engineering may be contaminated by impulsive noise, which is primarily characterized by sudden and rapid fluctuations in the measurement within a short period of time. Impulsive noise typically originates from sensor malfunctions, electromagnetic interference in measurement and control systems, or combustion oscillation, among other sources. Although not inherently indicative of a fault, this can potentially impact the robustness of the identification process. The present section enhances the PAST by incorporating the influence of weights. A surrogate modeling approach based on variable weight PAST (VWPAST) is proposed.

The new criterion function is established based on Eq. (18), as depicted in Eq. (29):

$$J(\mathbf{W}_k) = \sum_{t=1}^k \alpha^{k-t} w_k \| \boldsymbol{\xi}_t - \mathbf{W}_k \mathbf{W}_k^T \boldsymbol{\xi}_t \|^2, \quad (29)$$

The Mahalanobis distance will be employed in this study to establish the weight coefficient, and the weight  $w$  will be defined as follows:

$$w_k = \frac{1}{d_m^2(\mathbf{z}_k, \mathbf{Z}_{k-1})}, \quad (30)$$

The Mahalanobis distance between  $\mathbf{z}_k$  and  $\mathbf{Z}_{k-1}$ , denoted as  $d_m(\mathbf{z}_k, \mathbf{Z}_{k-1})$  [63], is being considered.  $\mathbf{Z}_{k-1} = [\mathbf{z}_1 \ \mathbf{z}_2 \ \dots \ \mathbf{z}_{k-1}] \in \mathbb{R}^{(m+j) \times (k-1)}$ .

$$d_m(\mathbf{z}_k, \mathbf{Z}_{k-1}) = \sqrt{(\mathbf{z}_k - \mathbf{Z}_{k-1,m}) \mathbf{S}^{-1} (\mathbf{z}_k - \mathbf{Z}_{k-1,m})^T}, \quad (31)$$

where the covariance between  $\mathbf{z}_k$  and  $\mathbf{Z}_{k-1,m}$ , denoted as  $\mathbf{S} = \text{Cov}(\mathbf{z}_k, \mathbf{Z}_{k-1,m})$ . The variable  $\mathbf{Z}_{k-1,m}$  represents the arithmetic mean of the set  $\mathbf{Z}_{k-1}$ ,  $\mathbf{Z}_{k-1,m} = \frac{1}{k-1} \sum_{i=1}^{k-1} \gamma^{k-i} \mathbf{z}_i$ ;  $\gamma$  is the forgetting factor,  $0.9 \leq \gamma \leq 1$ .

The data distribution at time  $k$  is considered inconsistent with the preceding data if the Mahalanobis distance between  $\mathbf{z}_k$  and  $\mathbf{Z}_{k-1}$  exhibits a sharp increase, thereby indicating an elevated probability of outliers in  $\mathbf{z}_k$ . The weight  $w$  assigned to update  $\mathbf{W}_k$  in this iteration will be reduced, ensuring the calculation's robustness.

The recurrence form for Eq. (21) will be transformed as follows:

$$\begin{aligned}
\mathbf{d}_t &= \mathbf{W}_{t-1}^T \boldsymbol{\xi}_t \\
\mathbf{g}_t &= \mathbf{K}_{t-1} \mathbf{d}_t \\
\mathbf{q}_t &= \mathbf{g}_t w_t / (\alpha + \mathbf{d}_t^T \mathbf{g}_t w_t), \\
\mathbf{K}_t &= [\mathbf{K}_{t-1} - \mathbf{q}_t \mathbf{g}_t^T] / \alpha, \\
\mathbf{e}_t &= \boldsymbol{\xi}_t - \mathbf{W}_{t-1} \mathbf{d}_t \\
\mathbf{W}_t &= \mathbf{W}_{t-1} + \mathbf{e}_t \mathbf{q}_t^T
\end{aligned} \tag{32}$$

The aforementioned is an enhancement of the PAST. The inclusion of weight in the recurrence process enhances the algorithm robustness.

#### 4. The unified framework for surrogate modeling

The present section presents a unified framework for generating a gas turbine surrogate model, as illustrated in Fig. 6.

The first step involves initializing the parameters  $\varphi_0, \mathbf{W}_0, \mathbf{P}_0, \mathbf{K}_0$  that require updating. Subsequently, the current input and measurements obtained from the sensor are received under closed-loop conditions and then normalized. The input and measurement data collected at every moment are utilized to update parameters within the algorithm based on the form in Fig. 4, ensuring that the surrogate model output is consistent with the actual measurements. The specific procedure involves updating parameter  $\varphi_k, \mathbf{P}_k$  through recursive least square method and the Markov parameter matrix  $\mathbf{M}_k$  is obtained. The parameters  $\mathbf{K}_k, \mathbf{W}_k$  are then updated using either the PAST method or VWPAST method, and finally  $\bar{\Gamma}_k = \mathbf{W}_k$  is set to extract the parameter matrices  $\mathbf{A}_k, \mathbf{B}_k, \mathbf{C}_k, \mathbf{K}_k$  of the model from the generalized observable matrix  $\bar{\Gamma}_k$ . Table 2. is the specific process.

#### 5. Results

##### 5.1. Surrogate model verification

Sections 5.1.1, 5.1.2 and 5.1.3 are conducted within simulation condition. The present study establishes a simulation performance

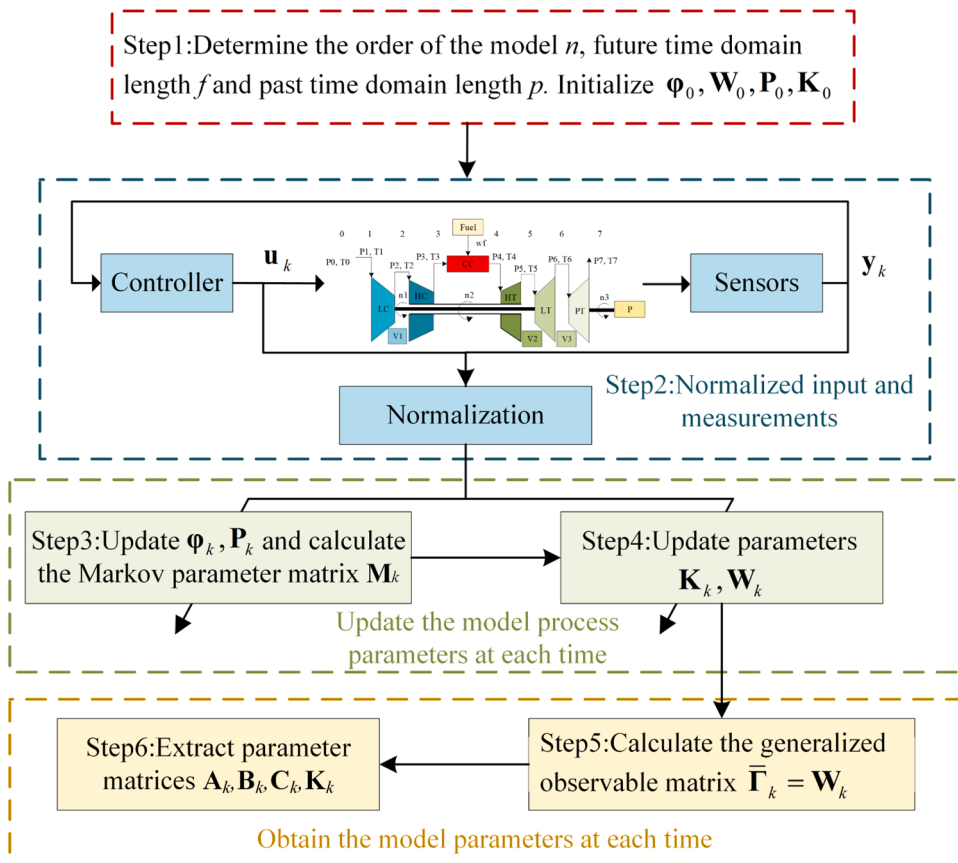


Fig. 6. The unified framework for gas turbine surrogate modeling.

**Table 2**

Process for generating gas turbine surrogate model.

**Step1:** Determine the order of the model  $n$ , future time domain length and past time domain length  $f=p=l$ . Determine the forgetting factors  $\alpha, \beta, \gamma$ . Initialize  $\varphi_0, \mathbf{W}_0$ ,  $\mathbf{P}_0, \mathbf{K}_0$ ,  $\mathbf{P}_0^{-1} = \mathbf{z}_{p,k} \mathbf{z}_{p,k}^T$ ,  $\varphi_0 = \Xi_{yz}(\Xi_{zz})^{-1}$ ,  $\mathbf{K}_0 = \mathbf{d}_0 \mathbf{d}_0^T$ ,  $\mathbf{W}_0$  is obtained by offline identification algorithm.

**Step2:** Normalize the input and measurements.

$$\mathbf{z}_k = \begin{bmatrix} \text{norm}(\mathbf{u}_k^T) \\ \text{norm}(\mathbf{y}_k^T) \end{bmatrix},$$

**Step3:** Update  $\varphi_k, \mathbf{P}_k$  and calculate the Markov parameter matrix  $\mathbf{M}_k$ .

$$\begin{aligned} \varphi_k &= \varphi_{k-1} + (\mathbf{y}_k - \varphi_{k-1} \mathbf{z}_{p,k}) \mathbf{Q}_k \\ \mathbf{Q}_k &= \frac{\mathbf{z}_{p,k}^T \mathbf{P}_{k-1}}{\beta + \mathbf{z}_{p,k}^T \mathbf{P}_{k-1} \mathbf{z}_{p,k}}, \\ \mathbf{P}_k &= \frac{(\mathbf{P}_{k-1} - \mathbf{P}_{k-1} \mathbf{z}_{p,k} \mathbf{Q}_k)}{\beta} \end{aligned} \quad (33)$$

$\mathbf{M}_{k,i} = \text{diag}(\mathbf{J}_1 \times R - i + 1, i - 1) \otimes \mathbf{h}_i + \mathbf{M}_{k,i-1}$ ,  $\mathbf{J}_m \times n$  is a  $m \times n$  matrix in which all elements are 1,  $\text{diag}(v, p)$  means that placing the elements of vector  $v$  on the  $p$ -th diagonal.  $p = 0$  denotes the main diagonal, with  $p > 0$  located above the main diagonal and  $p < 0$  located below it.

end

**Step4:** Update the parameter  $\mathbf{K}_k, \mathbf{W}_k$ .

PAST

$$\begin{aligned} \mathbf{d}_k &= \mathbf{W}_{k-1}^T \xi_k \\ \mathbf{g}_k &= \mathbf{K}_{k-1} \mathbf{d}_k \\ \mathbf{q}_k &= \mathbf{g}_k / (\alpha + \mathbf{d}_k^T \mathbf{g}_k), \\ \mathbf{K}_k &= [\mathbf{K}_{k-1} - \mathbf{q}_k \mathbf{g}_k^T] / \alpha \\ \mathbf{e}_k &= \xi_k - \mathbf{W}_{k-1} \mathbf{d}_k \end{aligned} \quad (34)$$

$$\begin{aligned} \sigma_k &= \| \mathbf{q}_k \|^2 \left( (1 + \| \mathbf{e}_k \|^2 \| \mathbf{q}_k \|^2)^{-1/2} - 1 \right) \\ \mathbf{e}'_k &= \sigma_k \mathbf{W}_{k-1} \mathbf{q}_k + (1 + \| \mathbf{q}_k \|^2) \mathbf{e}_k, \\ \mathbf{W}_k &= \mathbf{W}_{k-1} + \mathbf{e}'_k \mathbf{q}_k^T \end{aligned} \quad (35)$$

VWPAST

$$d_m(\mathbf{z}_k, \mathbf{Z}_{k-1}) = \sqrt{(\mathbf{z}_k - \mathbf{Z}_{k-1,m}) \mathbf{S}^{-1} (\mathbf{z}_k - \mathbf{Z}_{k-1,m})^T}, \quad (36)$$

$$w_k = \frac{1}{d_m^2(\mathbf{z}_k, \mathbf{Z}_{k-1})}, \quad (37)$$

$$\begin{aligned} \mathbf{d}_k &= \mathbf{W}_{k-1}^T \xi_k \\ \mathbf{g}_k &= \mathbf{K}_{k-1} \mathbf{d}_k \\ \mathbf{q}_k &= \mathbf{g}_k w_k / (\alpha + \mathbf{d}_k^T \mathbf{g}_k w_k), \\ \mathbf{K}_k &= [\mathbf{K}_{k-1} - \mathbf{q}_k \mathbf{g}_k^T] / \alpha \\ \mathbf{e}_k &= \xi_k - \mathbf{W}_{k-1} \mathbf{d}_k \end{aligned} \quad (38)$$

$$\begin{aligned} \sigma_k &= \| \mathbf{q}_k \|^2 \left( (1 + \| \mathbf{e}_k \|^2 \| \mathbf{q}_k \|^2)^{-1/2} - 1 \right) \\ \mathbf{e}'_k &= \sigma_k \mathbf{W}_{k-1} \mathbf{q}_k + (1 + \| \mathbf{q}_k \|^2) \mathbf{e}_k, \\ \mathbf{W}_k &= \mathbf{W}_{k-1} + \mathbf{e}'_k \mathbf{q}_k^T \end{aligned} \quad (39)$$

**Step5:** Calculate the extended observable matrix.

$$\bar{\Gamma}_{f,k} = \mathbf{W}_k, \quad (40)$$

**Step6:** Extract parameter matrices  $\mathbf{A}, \mathbf{B}, \mathbf{C}, \mathbf{K}$

$$\mathbf{C} = \bar{\Gamma}_{f,k}(1:m, :), \quad (41)$$

(continued on next page)

**Table 2** (continued)

$$\bar{\mathbf{B}} = \bar{\Gamma}_{f,k}^i \begin{bmatrix} \mathbf{C}\bar{\mathbf{B}} \\ \mathbf{C}\bar{\mathbf{A}}\bar{\mathbf{B}} \\ \vdots \\ \mathbf{C}\bar{\mathbf{A}}^{f-1}\bar{\mathbf{B}} \end{bmatrix}, \quad (42)$$

$$\mathbf{B} = \bar{\mathbf{B}}(:, 1:j)$$

$$\mathbf{K} = \bar{\mathbf{B}}(:, j+1:j+m)$$

$$\bar{\mathbf{A}} = \bar{\Gamma}_{f,k}^i(1:n(f-1), :) \bar{\Gamma}_{f,k}(n+1:nf, :)$$

$$\mathbf{A} = \bar{\mathbf{A}} + \mathbf{K}\mathbf{C}, \quad (43)$$

Repeat step 2- steps 6  
End

model for a three-shaft gas turbine to accurately replicate the operational process of a gas turbine. The data presented in [Section 5.1.4](#) represents actual measurements obtained from bench experiment of a gas turbine.

The gas turbine performance model serves as the simulation model. Under simulation conditions, it assumes that external factors are solely influenced by temperature and pressure, with boundary conditions set at an atmospheric temperature of 288.15 K and atmospheric pressure of 101.325 kPa. The simulation step size is defined as 0.01, while the numerical calculation method employed is Runge-Kutta algorithm of order 4. For the specific equations used in the modeling process, the reader is referred to the paper [[64](#)].

The variables were normalized in this study to prevent the occurrence of ill-conditioned matrices during the establishment of the surrogate model. The equation is as follows:

$$\mathbf{x}_{norm} = \frac{\mathbf{x} - \mathbf{x}_{min}}{\mathbf{x}_{max} - \mathbf{x}_{min}}, \quad (44)$$

where the normalized data is denoted as  $\mathbf{x}_{norm}$ . The minimum and maximum values of the sequence are represented by  $\mathbf{x}_{min}$  and  $\mathbf{x}_{max}$  respectively.

### 5.1.1. Analysis of modeling results for rated steady-state condition

The modeling results for rated steady-state condition are first analyzed. The selected model input is fuel flow  $w_f$ . Given a rated power signal, the white noise  $e_k$  has a mean of 0 and a variance of 0.05. [Fig. 7](#) illustrates the gas turbine fuel flow at present:

The vertical coordinate is the fuel flow for rated condition. With the given hyperparameters in the modeling process, including a model order of  $n = 7$  (The selection of model order in this research is grounded on [Assumption 1](#), detailed in [Section 3.2](#). This choice was reached after numerous trials, aiming to maintain the model order as minimal as feasible while ensuring the accuracy of the model), a past and future time domain size of  $p = f = 25$ , and forgetting factors of  $\alpha = \beta = \gamma = 0.995$ , please refer to Step 1 in the flowchart for initializing the variables in the recursion process.

The modulus length of the eigenvalue of the system matrix  $\bar{\mathbf{A}}$  is obtained at each step during the modeling process in order to observe changes in the surrogate model, as depicted in [Fig. 8](#).

In [Fig. 8](#), the vertical coordinate denotes the modulus length of the eigenvalue (Eig) of the model system matrix. The modulus length of eigenvalues is  $<1$ , indicating that the model is asymptotically stable. Moreover, the eigenvalue gradually converges to a constant value from its initial dynamic change, implying that the surrogate model progressively reaches a stable state through recurrence. The selected model outputs include the outlet temperature of the high-pressure compressor (T3), the outlet temperature of the low-pressure turbine (T6), the speed of the low-pressure compressor (n1), the speed of the high-pressure compressor (n2), and the outlet pressure of the low-pressure turbine (P6). [Fig. 9](#) is the comparison between the surrogate model output and the performance model output, with the blue line representing the surrogate model output and the red line representing the performance model output.

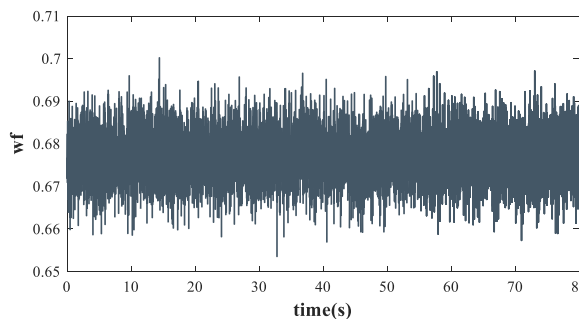


**Fig. 7.** Fuel flow for rated condition.

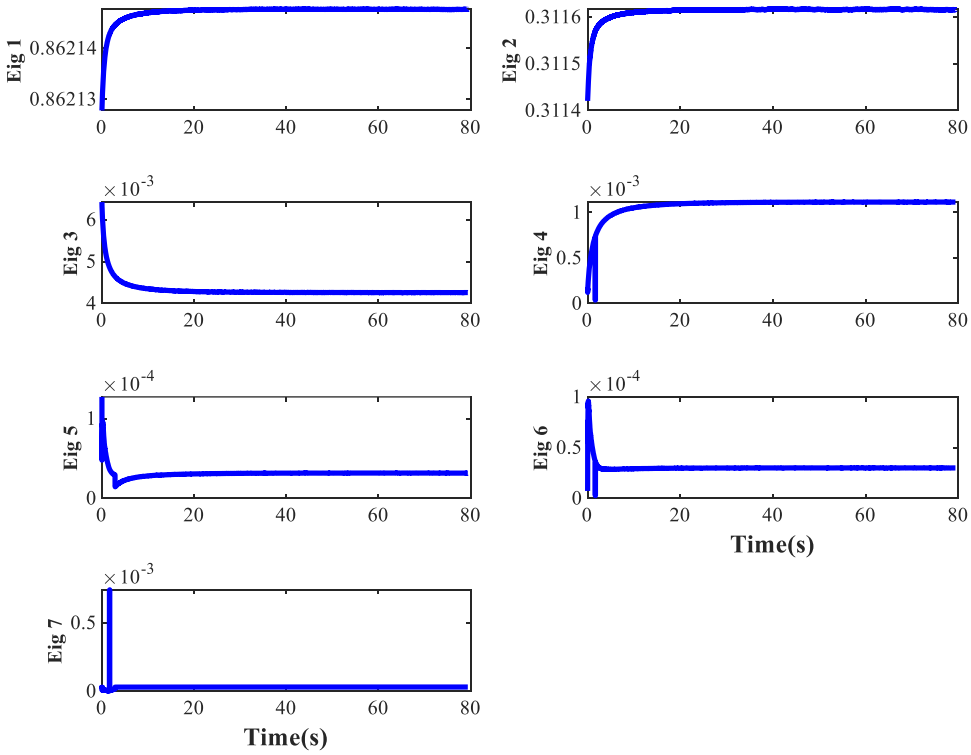


**Fig. 8.** The modulus length of the model eigenvalue for rated condition.

The fit between the surrogate model output and the performance model output is deemed satisfactory, as evidenced by [Fig. 9](#). The discrepancy between the surrogate model output and the performance model output is quantified using the following methodology:

$$\text{Error} = \frac{\hat{y}_i - y_i}{y_i} \times 100\% \quad (45)$$

where  $\hat{y}_i$  represents each output of surrogate model at the  $i$ -th time point, and  $y_i$  represents each output of performance model at the  $i$ -th time point.

The accuracy and convergence speed of the model are generally influenced by the choice of forgetting factor. [Fig. 10](#) is the error between the surrogate model output and the performance model output for different forgetting factors (FF).

The progression of recursion in [Fig. 10](#) demonstrates a gradual decrease and eventual stabilization of the error between the surrogate model output and performance model output. This pattern aligns with the change in eigenvalue, indicating a correlation with the selection of forgetting factor during recursion. The smaller the value of the forgetting factor, the higher the convergence rate of the model. Taking n1 as an example, it can be observed that when the forgetting factor is set to 0.990, the model achieves its fastest convergence rate; whereas with a forgetting factor of 0.999, the convergence rate becomes significantly slower. The robustness of the identification decreases when the forgetting factor is too small, as indicated by an increase in the error between the surrogate model output and performance model output at specific points, such as when using a forgetting factor of 0.990 or 0.992.

The mean steady-state error of the model was analyzed and quantified using the mean absolute percentage error (MAPE) for different forgetting factors. The calculation equation is as follows:

$$\text{MAPE} = \frac{1}{n} \sum_{i=1}^n \left| \frac{\hat{y}_i - y_i}{y_i} \right| \times 100\% \quad (46)$$

The results in [Table 3](#) demonstrate a decrease in MAPE as the forgetting factor increases; however, this improvement comes at the expense of slower convergence speed. To strike a balance between model accuracy and convergence speed, the forgetting factor of 0.995 was chosen for this study, ensuring a steady-state error below 0.0056 %.

The analysis of modeling results for the rated steady-state working condition reveals that the output of established surrogate model based on the Markov-PAST effectively tracks gas turbine measurements in steady-state conditions, while ensuring robustness and convergence speed through appropriate selection of forgetting factors.

### 5.1.2. Analysis of modeling results in the presence of impulsive noise

The operation of gas turbines in practical engineering is occasionally disrupted by impulsive noise, which manifests as sudden

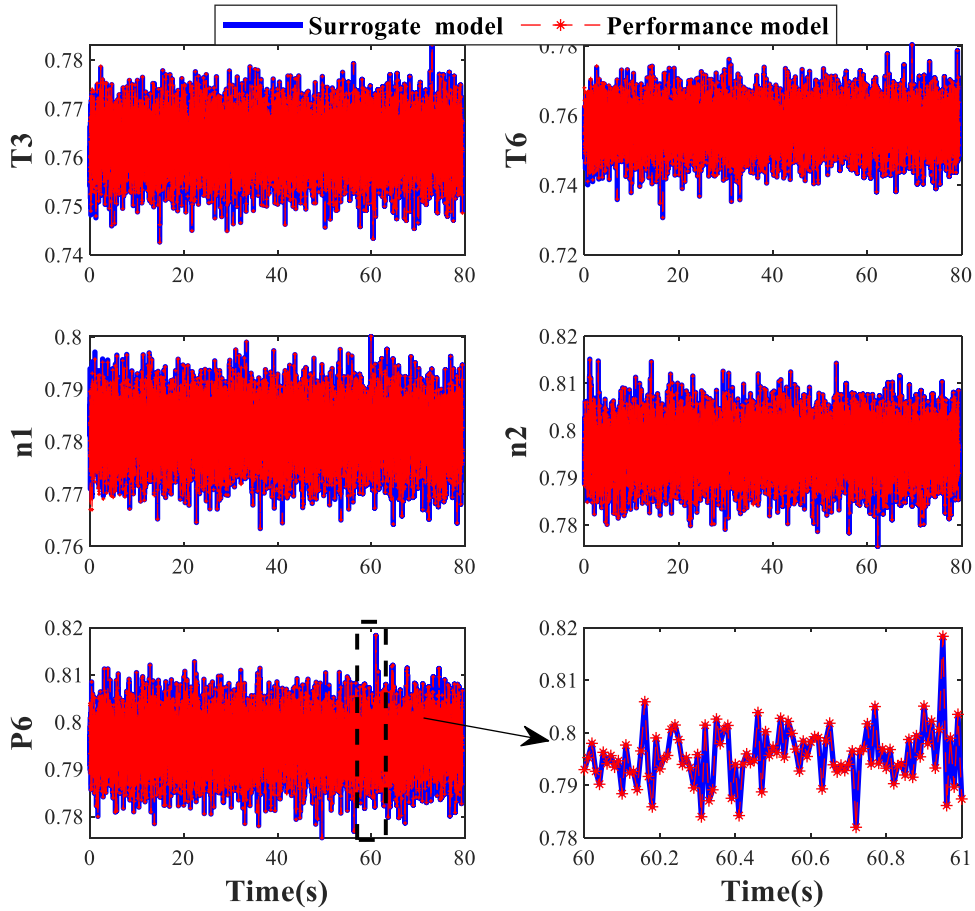


**Fig. 9.** Comparison of surrogate model output and performance model output for rated condition.

fluctuations in measurements within a short time frame. Although not indicative of a fault, this phenomenon can impact identification accuracy and diminish robustness. The present study addresses this issue by incorporating the impact of weight into the recurrent process of the original algorithm, thereby proposing the VWPAST algorithm. The measurement data in Section 5.1.1 has been augmented with an impulsive noise, characterized by a zero mean and a variance of 0.5, to validate the VWPAST algorithm.

Fig. 11 is the output of the surrogate model obtained using the PAST and VWPAST, respectively.

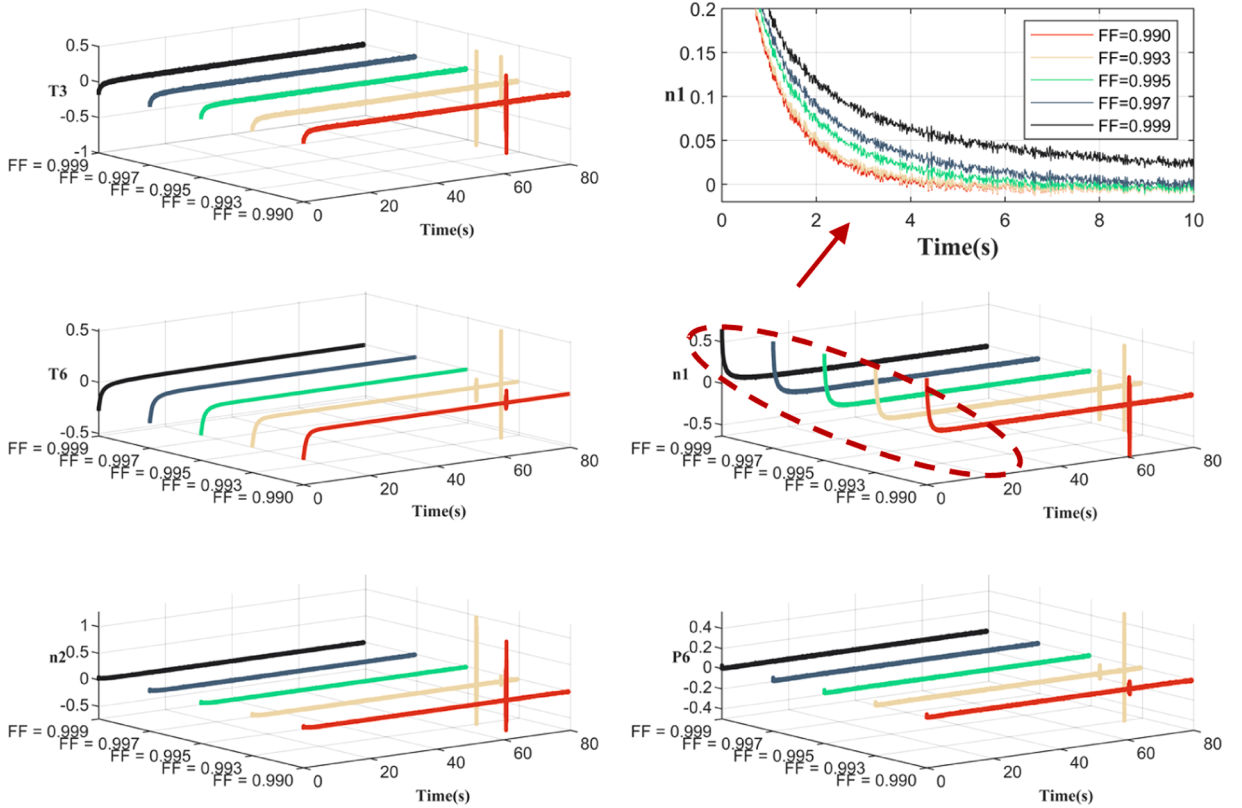
The analysis of Fig. 11 reveals that both methods exhibit a certain level of output value mutation when subjected to impulsive noise. Taking P6 as an example, the enlarged figure demonstrates that the VWPAST exhibits smaller output value mutations compared to the PAST. The above results demonstrate that the output of the surrogate model established by VWPAST can contribute to impulsive noise reduction to a certain extent.

Fig. 12 is the weight variation in the iterative process with the introduction of impulsive noise. The vertical coordinate is the change in weight  $w$ :

The weight coefficient decreases to nearly 0, as depicted in Fig. 12, indicating a deviation of the Mahalanobis distance from the original distribution for the measurement data at this particular time due to the introduction of impulsive noise. Consequently, there is a sudden increase in the Mahalanobis distance between the two, leading to an abrupt drop in weight. Subsequently, when the impulsive noise subsides, the weight gradually reverts back to its original value.

The VWPAST is utilized in the process to obtain the eigenvalue modulus length of the system matrix  $\bar{A}$  at each step of the recurrence process, enabling observation of model changes throughout the recurrence process, the results are compared with the PAST, as depicted in Fig. 13.

The vertical coordinate is the change of the eigenvalue modulus length of the eigenvalues of the model system matrix  $\bar{A}$  obtained by using the two methods. The eigenvalue of the PAST method exhibits a sudden change at the moment when impulsive noise occurs, leading to a decrease in identification robustness. However, with the passage of time, it gradually reverts back to its original value. The convergence speed of the main eigenvalue using the VWPAST method is relatively slow due to the presence of weight in the recurrence process. However, this weight plays a crucial role by minimizing its impact during impulsive noise occurrences, thereby mitigating mutations and allowing for a consistent trend towards gradual convergence to a specific value. The fluctuation of small eigenvalues becomes irregular, however, due to their relatively low contribution rate to the system matrix, it will not significantly impact the



**Fig. 10.** Error of surrogate model output and performance model output for different forgetting factors (%).

**Table 3**

Steady-state error of model with different forgetting factors (%).

Variables FF	T3	T6	n1	n2	P6
0.990	0.0055	0.0072	0.0028	0.0066	0.0050
0.992	0.0046	0.0059	0.0039	0.0062	0.0036
0.995	0.0028	0.0056	0.0024	0.0054	0.0024
0.997	0.0016	0.0052	0.0016	0.0049	0.0021
0.999	0.0004	0.0045	0.0011	0.0042	0.0005

overall identification process.

#### 5.1.3. Analysis of modeling results for variable working conditions

The applicability of the surrogate model building method proposed in this study for variable working conditions is verified by utilizing a performance model to simulate the operation of a gas turbine within a specific operating range.

The power signal depicted in Fig. 14 is presented in this working diagram. The working diagram encompasses the operational conditions of five processes, simulating the condition of load lifting and load reduction during actual operation.

The vertical coordinate is the demand power signal. The comparison between the surrogate model output and the performance model output for different working conditions is illustrated in Fig. 15.

As depicted in Fig. 15, the surrogate model output and performance model output exhibit a high degree of conformity even for variable working conditions. The error between the two is quantified by Eq. (35), as illustrated in Fig. 16.

The error gradually stabilizes from the initial dynamic change, similar to the rated working condition, as depicted in Fig. 16. However, during the working condition switching stage, the error increases to a certain extent. This increase is particularly significant when there is a large span in the working condition switching. For instance, as illustrated by the red box in the figure, when the working condition transitions from 0.6 to 0.9 and rapidly decreases back to 0.5, there is a dramatic surge in error magnitude. The specific changes in error are presented in Table 4.

The MAPE between the surrogate model output and the performance model output is observed to be below 0.275 % for variable working conditions, as depicted in Table 4. Notably, the maximum error of 2.038 % occurs when there is a wide range of changes in the

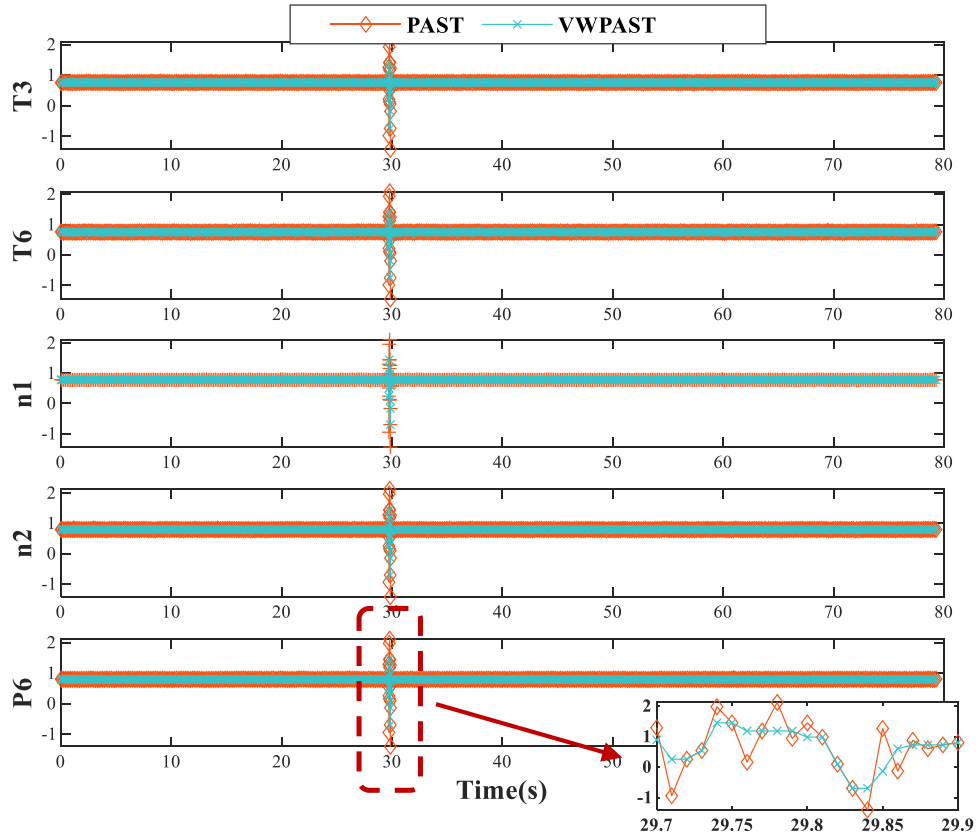


**Fig. 11.** Comparison of model output based on PAST and VWPAST when adding impulsive noise.

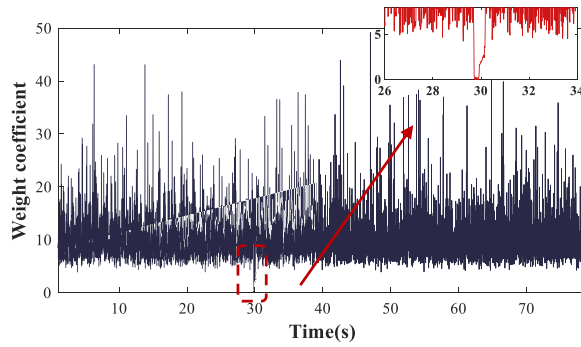


**Fig. 12.** The change of weight coefficient when adding impulsive noise.

working conditions.

#### 5.1.4. Analysis of modeling results from bench experiment of an actual gas turbine

In order to validate the practical applicability of the proposed surrogate model, this study utilized operational data from a specific three-shaft gas turbine in a bench experiment and employed the surrogate model for real-time tracking of measurement data. The experiment was conducted under standard atmospheric pressure. Fig. 17 illustrates the variations in ambient temperature and given power during this bench test.

The vertical coordinate is the atmospheric temperature and the given power signal, which are the boundary conditions of gas turbine operation, and the horizontal coordinate is the running time of this bench experiment. Fig. 18 is the results of tracking actual gas turbine operation data using the surrogate model established.

The figure demonstrates that the output of the surrogate model remains consistent with the actual gas turbine measurement even when subjected to variable ambient temperature and operating conditions. Fig. 19 visually illustrates the discrepancy between the two.

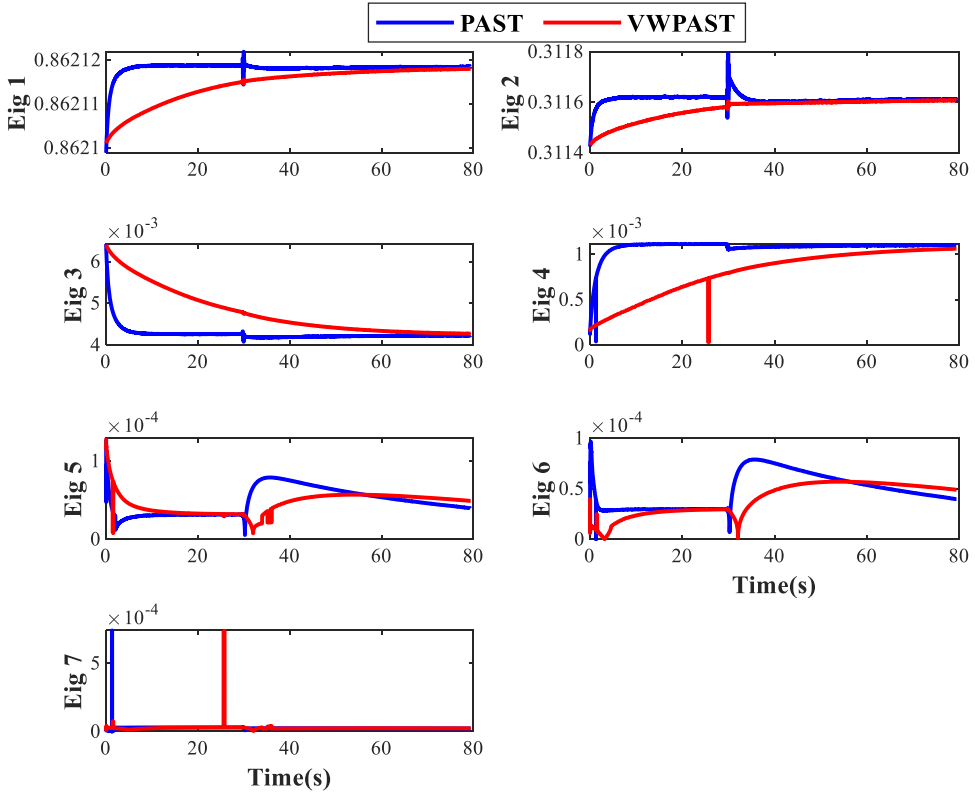


**Fig. 13.** Comparison of eigenvalue modulus length changes between PAST and VWPAST when adding impulsive noise.

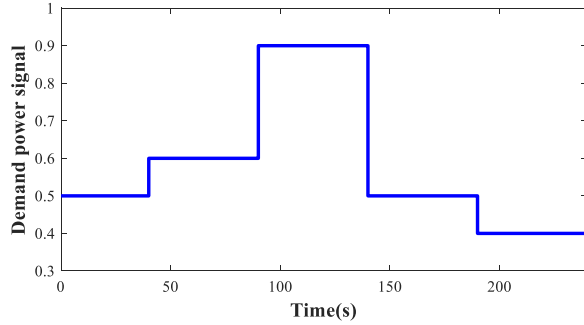


**Fig. 14.** Demand power signal for variable working conditions.

The error between the surrogate model output and the actual measurements of the gas turbine are observed to be consistently within a low range, as depicted in Fig. 19. The position where the error increases is located at the point of switching working conditions, which is similar to the variable working conditions in simulation. The error will tend to escalate under low operating conditions; however, overall, it remains within an acceptable range. These errors are quantified using two indices: maximum relative error and MAPE, which are presented in Table 5.

The results in Table 5 demonstrate that the maximum relative error between the output of the surrogate model and the measurements of the actual gas turbine is 0.549 %, and MAPE is within 0.083 %, thereby substantiating the established model's credibility in real engineering application.

## 5.2. Application of surrogate model for condition monitoring

The surrogate model established in this study is mainly oriented to gas turbine condition monitoring. Since the established surrogate model can be consistent with the behavior of the actual gas turbine, the model parameters of the surrogate model will also change correspondingly when the gas turbine is abnormal. If the feature quantity of the model structure evolution can be extracted, the

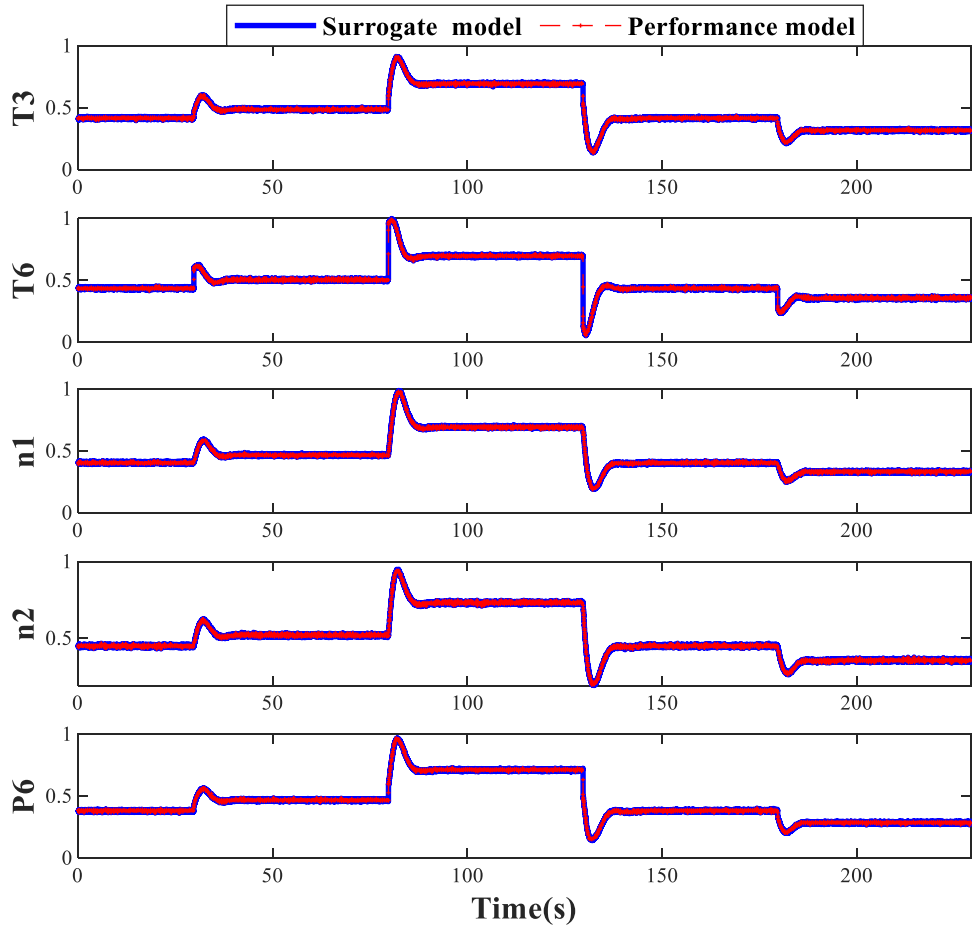


**Fig. 15.** Comparison of surrogate model output and performance model output for variable working conditions.

real-time feedback on the gas turbine condition can be obtained. The objective of this section is to utilize changes in model parameters to achieve condition monitoring of gas turbines under three typical operating conditions.

#### 5.2.1. Sudden fault detection

This section will briefly discuss an instance of a sudden failure in a gas turbine. The term "sudden failure" primarily refers to the damage inflicted on the gas turbine by external or internal factors during a specific time period. This is predominantly characterized by abrupt variations in efficiency and flow rate within the gas path system, consequently leading to alterations in the operational characteristics of the gas turbine at that particular moment [65]. Based on this characteristic, the performance model of a gas turbine is utilized in this study to simulate the condition when the compressor efficiency abruptly decreases to 95 % of its normal condition [66], as depicted in Fig. 20, the vertical coordinate is the decrease of compressor efficiency. Fig. 21 is fuel flow  $wf$  and measurements of the gas turbine.

Fig. 21 illustrates that when the fault was introduced at 20 s, due to the closed-loop control strategy, the control system had to increase the fuel flow for the gas turbine to maintain its original output power when a decrease in efficiency. Consequently, this affected other measurements. By employing the method proposed in this study and using the PAST as an example, we obtained changes in eigenvalue modulus length of the system matrix under these conditions to observe how sudden faults impact the model, as depicted in Fig. 22.

The observation from Fig. 22 reveals that at 20 s, similar to the model changes in a normal condition, the primary eigenvalue underwent dynamic variations initially and gradually reached stability. When a fault occurred, the primary eigenvalue exhibited an abrupt change and progressively converged towards another fixed value with increasing running time, indicating a modification in the model structure at the time of fault occurrence. The mapping relationship between model inputs and outputs has consequently undergone alteration and reconstruction. The change in the model structure signifies a deviation of the gas turbine from its normal operating condition. Based on this characteristic, fault detection of the gas turbine can be conducted.

The eigenvalues of the system matrix reflect the characteristics of the model itself, but in practical application, the change of the eigenvalue is limited to a small range, so it is difficult to capture this change, and it is necessary to find an additional feature to

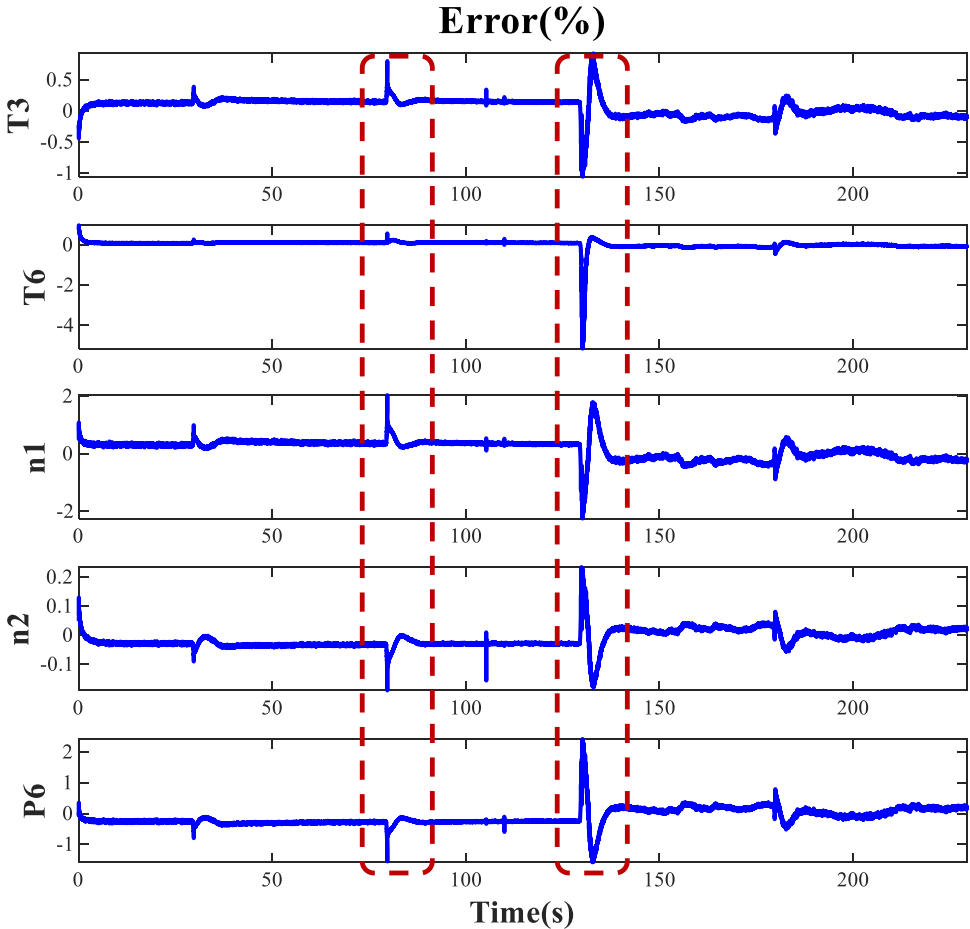


**Fig. 16.** Error between surrogate model output and performance model output for varying working conditions.

**Table 4**

Error between surrogate model output and performance model output for variable working conditions (%).

Variables	T3	T6	n1	n2	P6
MAPE	0.125	0.068	0.275	0.025	0.231
Error <sub>max</sub>	1.152	0.801	2.038	0.206	1.888

represent the change of the model. According to the analysis in [Section 3.2](#), Markov parameter vector  $\varphi = [\mathbf{C}\bar{\mathbf{B}} \quad \mathbf{C}\bar{\mathbf{A}}\bar{\mathbf{B}} \quad \dots \quad \mathbf{C}\bar{\mathbf{A}}^{p-1}\bar{\mathbf{B}}]$  in the modeling process contains the information of model parameters  $\mathbf{A}, \mathbf{B}, \mathbf{C}, \mathbf{K}$ , whose physical significance indicates the influence of  $p$  time domain data before  $k$  time on the current output. Therefore,  $\varphi$  is selected in this section as the feature quantity of model parameters evolution, which is called model mismatch feature in this study (This statement requires mathematical proof process, which will be reflected in the subsequent research, but it is not the main content of this study, which is only for demonstration).

$\varphi$  is a  $m \times (m + 1)p$  matrix, which can be regarded as a multidimensional distribution,  $m$  is the measurement dimension. We use Wasserstein distance [67] to quantify the distributed distance between normal and actual gas turbine, and the calculation equation of Wasserstein distance is as follows:

$$w(a, h) = \left( \inf_{\gamma \in \Pi(a, h)} \int \int \gamma(\mathbf{x}, \mathbf{y}) \| \mathbf{x} - \mathbf{y} \|^s d\mathbf{x} d\mathbf{y} \right)^{1/s} = \left( \inf_{\gamma \in \Pi(a, h)} E_{(\mathbf{x}, \mathbf{y}) \sim \gamma(\mathbf{x}, \mathbf{y})} [\| \mathbf{x} - \mathbf{y} \|^s] \right)^{1/s}, \quad (47)$$

where  $h$  denotes the distribution of feature in normal gas turbine,  $a$  represents that of the distribution of feature in actual gas turbine,  $s$  is the order. When  $s=1$ , Wasserstein distance is employed to compute the distance between two vectors with identical dimensions. The Wasserstein distance is employed for computing the distance between two matrices or tensors of identical dimensions when  $s=2$ . The Wasserstein distance is employed to compute the dissimilarity between two shapes of different dimensions when the order of  $s$  is higher dimensional. Considering that the mismatch feature takes the form of a matrix,  $s=2$  is selected for computation in this study.

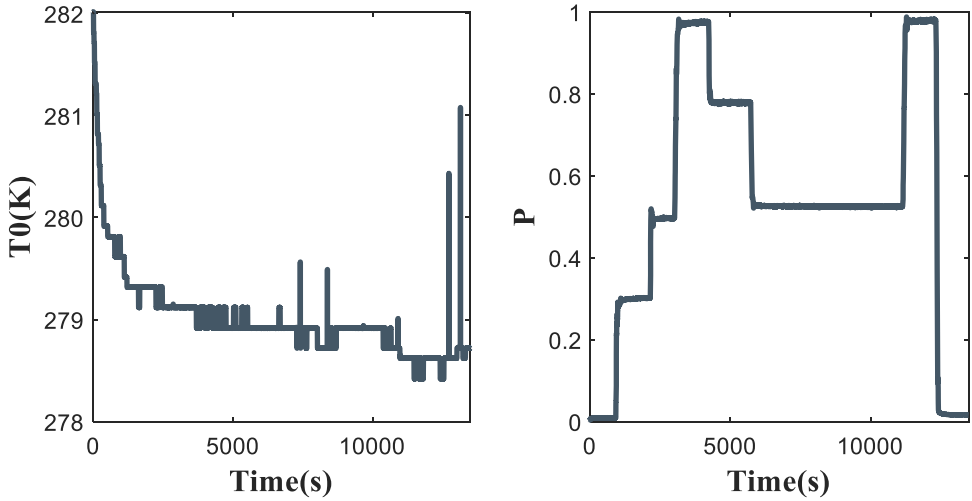


**Fig. 17.** Ambient temperature and given power of three-shaft gas turbine bench experiment.

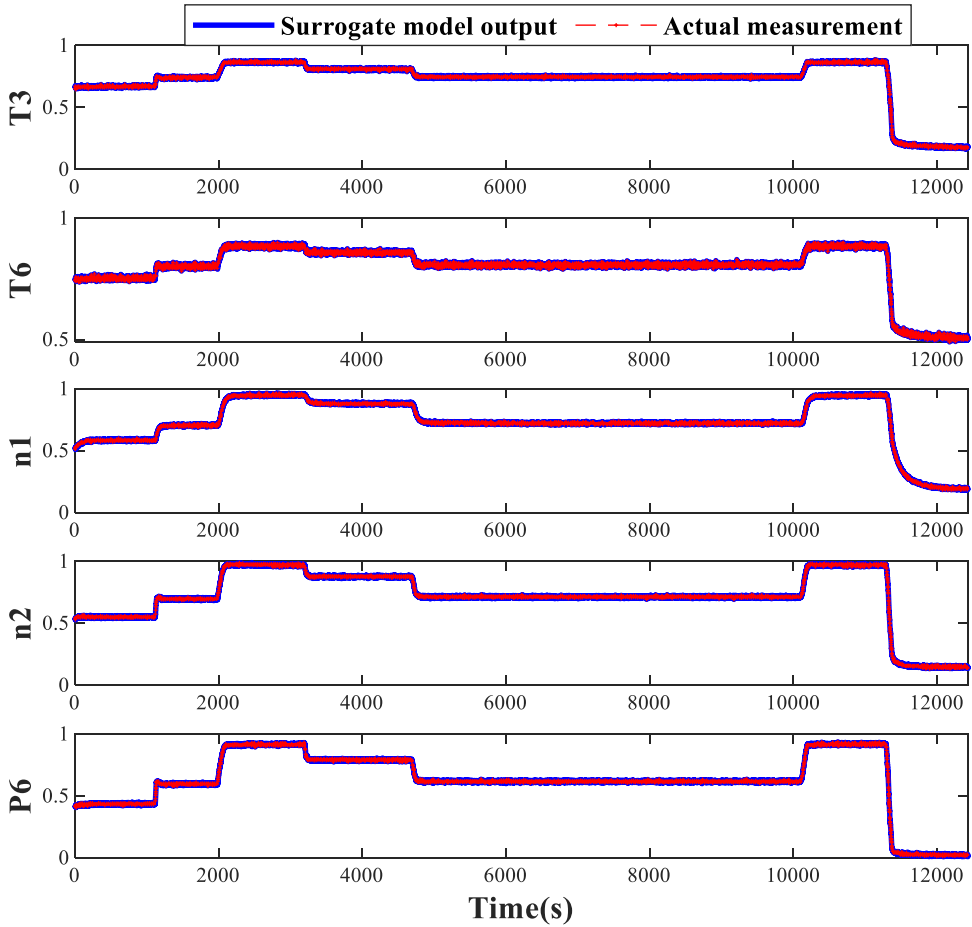


**Fig. 18.** Comparison of surrogate model output and actual measurements.

[Fig. 23](#) is the Wasserstein distance of model mismatch feature change in the case shown in [Fig. 21](#):

As illustrated in the figure above, the Wasserstein distance stays approximately at 0 for the first 20 s, suggesting that the gas turbine condition is nearly normal during this interval. At 20 s, the gas turbine experienced a sudden failure, coinciding with a sharp increase in the Wasserstein distance. This indicates a shift in the model structure, moving away from the normal range and highlighting

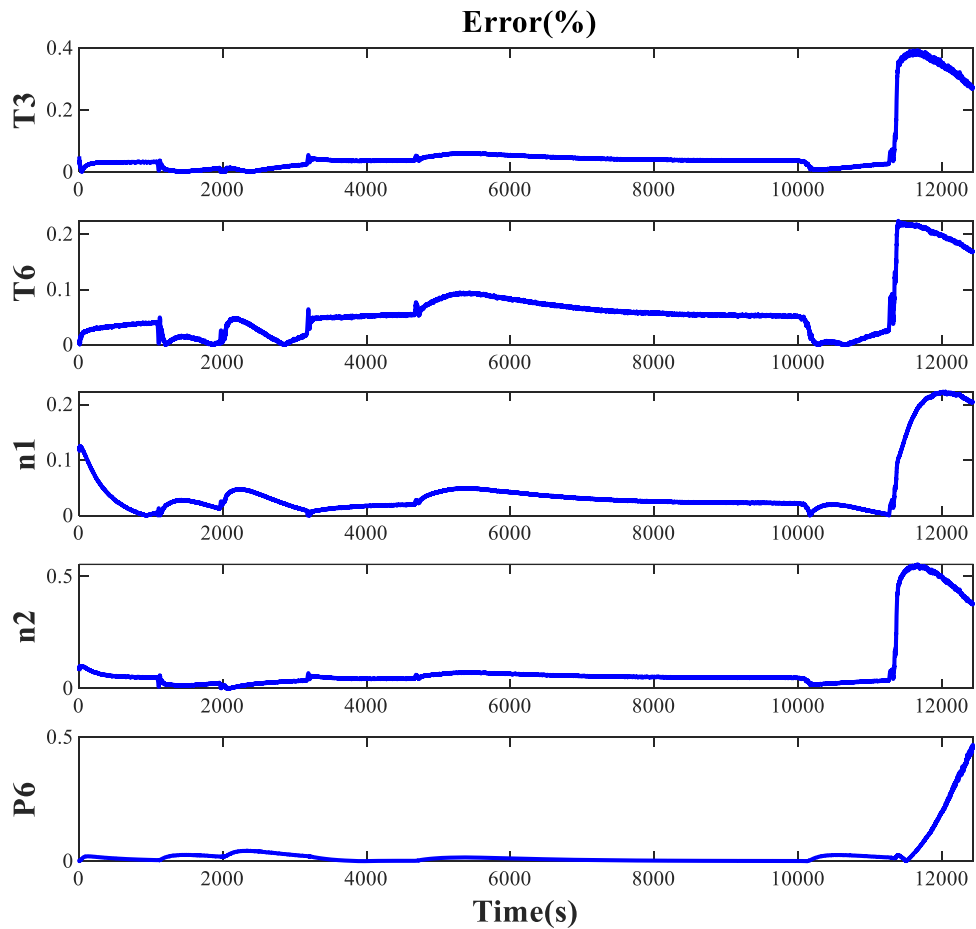


**Fig. 19.** Error between surrogate model output and actual measurements.

**Table 5**

Error between surrogate model output and actual measurements in bench experiment (%).

Variables	T3	T6	n1	n2	P6
MAPE	0.060	0.059	0.041	0.083	0.025
Error <sub>max</sub>	0.393	0.224	0.220	0.549	0.458

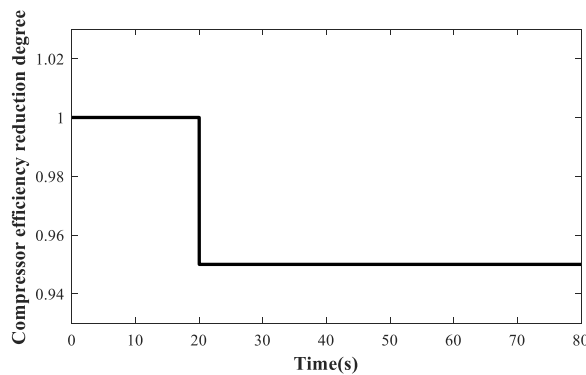


**Fig. 20.** Degree of decrease in low-pressure compressor efficiency for sudden failure.

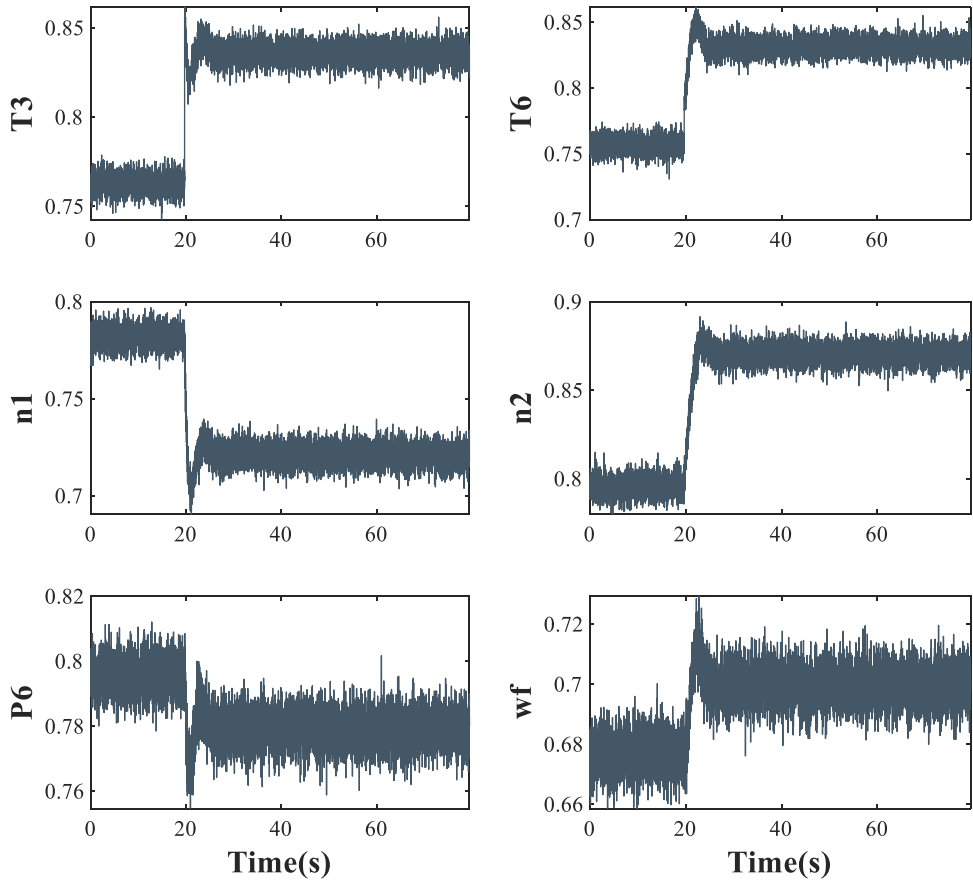


**Fig. 21.** Changes in input and measurement for sudden failure.

abnormal condition of the gas turbine. Moreover, this alteration is more pronounced than changes in the model eigenvalue, demonstrating broader applicability in condition monitoring of gas turbine.

### 5.2.2. Gradational degradation assessment

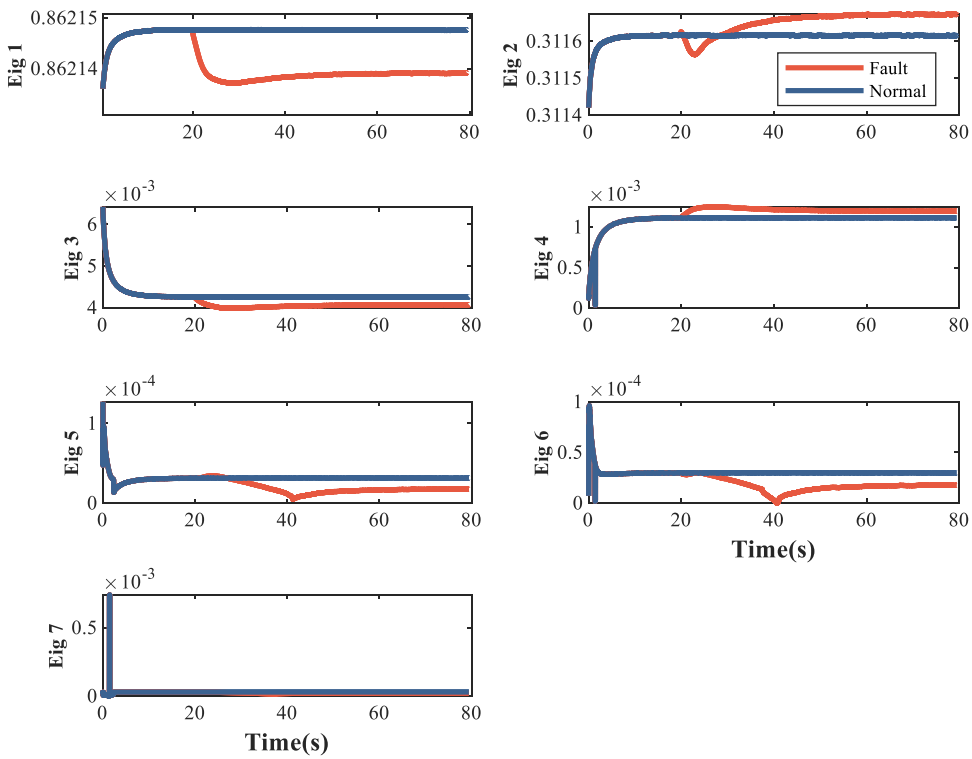
The present section will examine the alterations in the model that occur during the progressive degradation of a gas turbine. The degradation of gas turbines primarily encompasses compressor fouling, blade erosion and corrosion, and increased blade tip clearance. These failures do not immediately render the gas turbine inoperable. Instead, they gradually diminish the performance of the gas turbine, leading to heightened fuel consumption and reduced efficiency. In severe cases, these issues can ultimately result in a complete failure of the gas turbine [68]. The degradation is primarily manifested by the gradual degradation of performance variables (flow and efficiency) in gas turbines, which can be categorized into exponential and linear degradation [69]. In order to observe the model parameters changes under degradation, this section presents a case study on the linear decline of compressor efficiency. The decline in compressor efficiency initiates at 20 s and gradually reaches 95 % of its normal condition, as illustrated in Fig. 24, the vertical coordinate is the decrease of compressor efficiency.

Fig. 25 is the changes of measurements and fuel flow in the linear degradation condition.

Fig. 25 demonstrates that in the event of a linear degradation in compressor efficiency, resembling a sudden failure, the control system must increase fuel flow to ensure constant output power while causing changes in other measurements. In the degradation condition, this study proposes employing the method to obtain the change in eigenvalue modulus length of system matrix  $\bar{A}$ , as depicted in Fig. 26.

The change in the model eigenvalue observed in Fig. 26 indicates that, during degradation, the model structure gradually deviates from its original condition. The feedback information of the model also indicates a gradual change in the condition of the gas turbine. Similar to Section 5.2.1, Fig. 27 illustrates the Wasserstein distance change of model mismatch feature between the normal and the actual condition of gas turbine.

The figure clearly shows that the Wasserstein distance begins to increase at 20 s, signaling that the gas turbine is progressively moving away from its normal operating range. This observation enables the implementation of predefined maintenance strategies based on the extent of deviation, thereby ensuring safe functionality of gas turbines.



**Fig. 22.** Change of model eigenvalue modulus length for sudden failure.

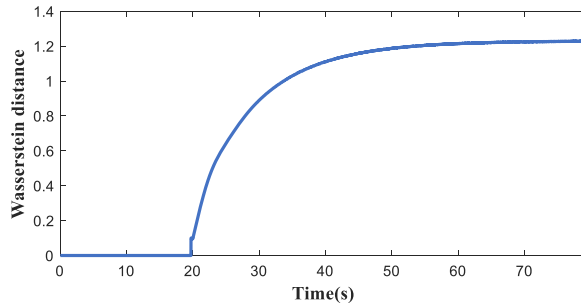


**Fig. 23.** Wasserstein distance of model mismatch feature distribution for sudden fault.

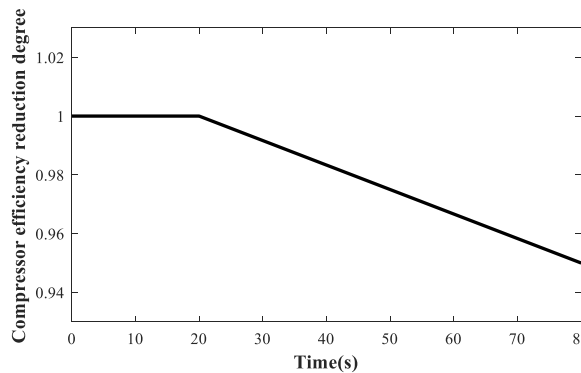


**Fig. 24.** Degree of decrease in low-pressure compressor efficiency for gradual degradation.

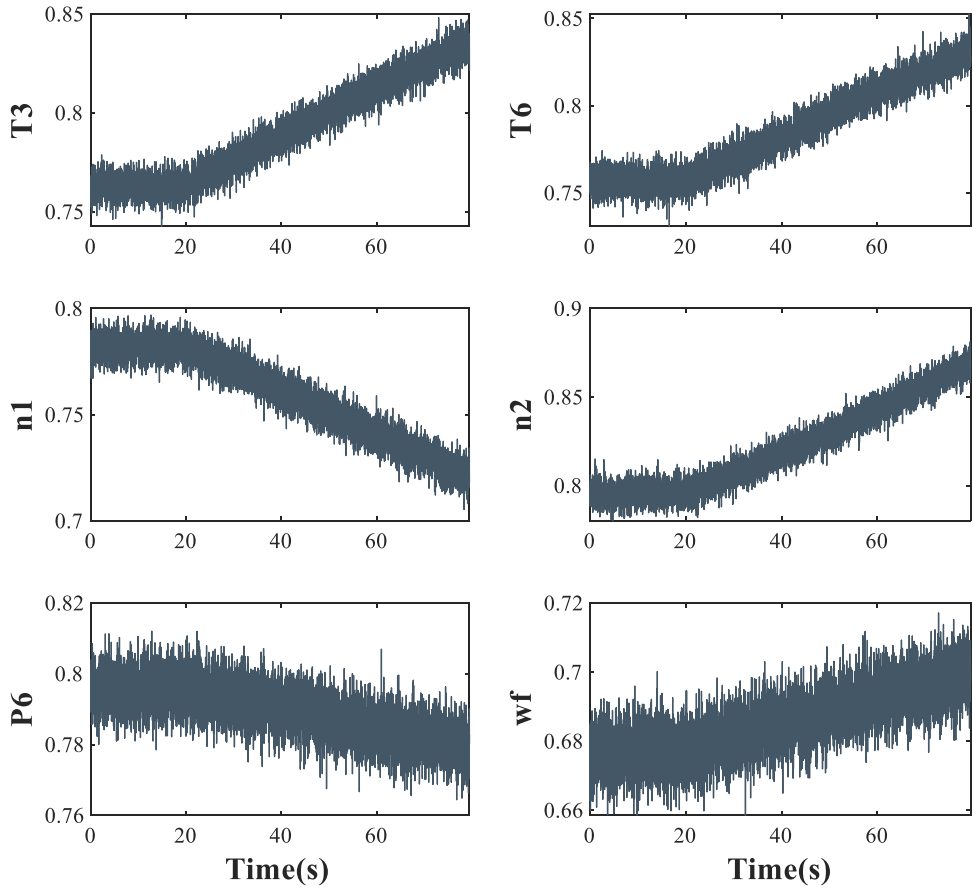


**Fig. 25.** Changes in input and measurement under gradual degradation.

#### 5.2.3. Sudden fault detection with impulsive noise

Drawing on the actual gas turbine operational data presented in [Section 5.1.4](#), this section introduces a simulation of a sudden fault and impulsive noise to attest to the effectiveness of the VWPAST in improving algorithm robustness within engineering application. The operational data, after the introduction of impulsive noise and sudden failure, are detailed as follows:

[Fig. 28](#) illustrates an instance where impulsive noise initially appears, typically manifested as fluctuations in the collected signal. These fluctuations can be attributed to various factors, such as gas turbine sensor malfunctions or electromagnetic interference. It is important to note that these disturbances are not indicative of an inherent fault in the gas turbine. However, they can lead to false alarm in fault detection and might even result in failure to converge subsequently of algorithm. Over time, a sudden failure emerged, a common occurrence in practical engineering. [Fig. 29](#) is the comparison of using VWPAST and PAST to detect the faults shown in the case shown in [Fig. 28](#):

[Fig. 29](#) illustrates that in the presence of impulsive noise, the Wasserstein distance associated with the PAST sharply rises to a value near 3000 s, in contrast to the VWPAST, which exhibits only minor fluctuations. This suggests that the VWPAST algorithm retains considerable robustness against impulsive noise, leading to a lower false alarm rate in practical application. Additionally, the VWPAST demonstrates the capability to accurately detect sudden failures though its convergence speed is somewhat slower compared to the PAST. This presents an area for improvement in future research endeavors.

In summary, the surrogate model established in this study contains actual gas turbine condition information, which can be applied to the field of gas turbine condition monitoring. By using the changes of model parameters, the feedback of gas turbine condition can be accurately obtained in the process of gas turbine sudden failure and gradual degradation, which strongly supports the development of gas turbine digital twin and realize bidirectional communication of gas turbine digital twin.

## 6. Conclusions

This paper establishes a surrogate model based on a Markov-PAST approach for gas turbine condition monitoring, which can be instrumental in the development of gas turbine digital twin. Utilizing the linear model, a Markov parameter matrix is constructed to derive the observation vector. The signal subspace, corresponding to the autocorrelation matrix of the observation vector, is determined through the PAST. This subspace serves as the equivalent of a generalized observable matrix, enabling the online identification

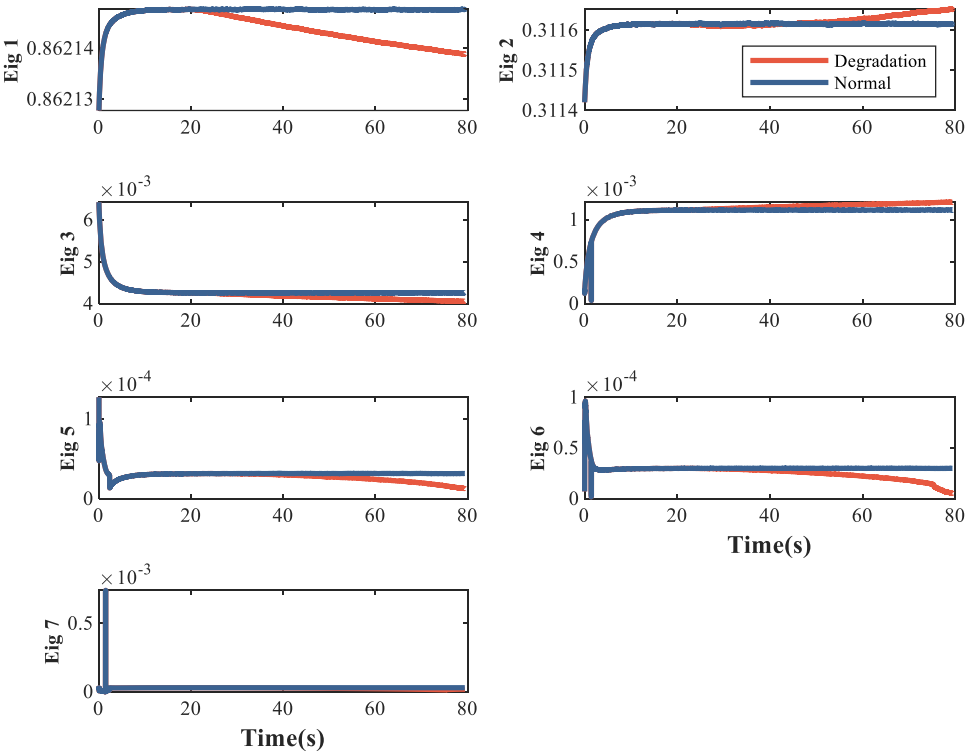


Fig. 26. Change of model eigenvalue modulus length under gradual degradation.

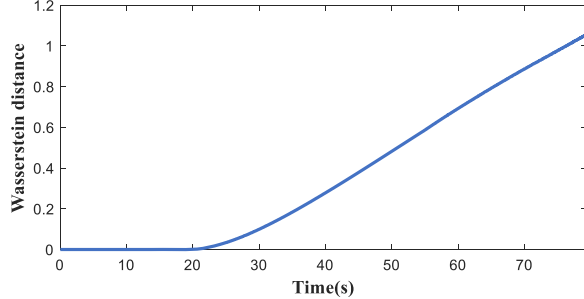
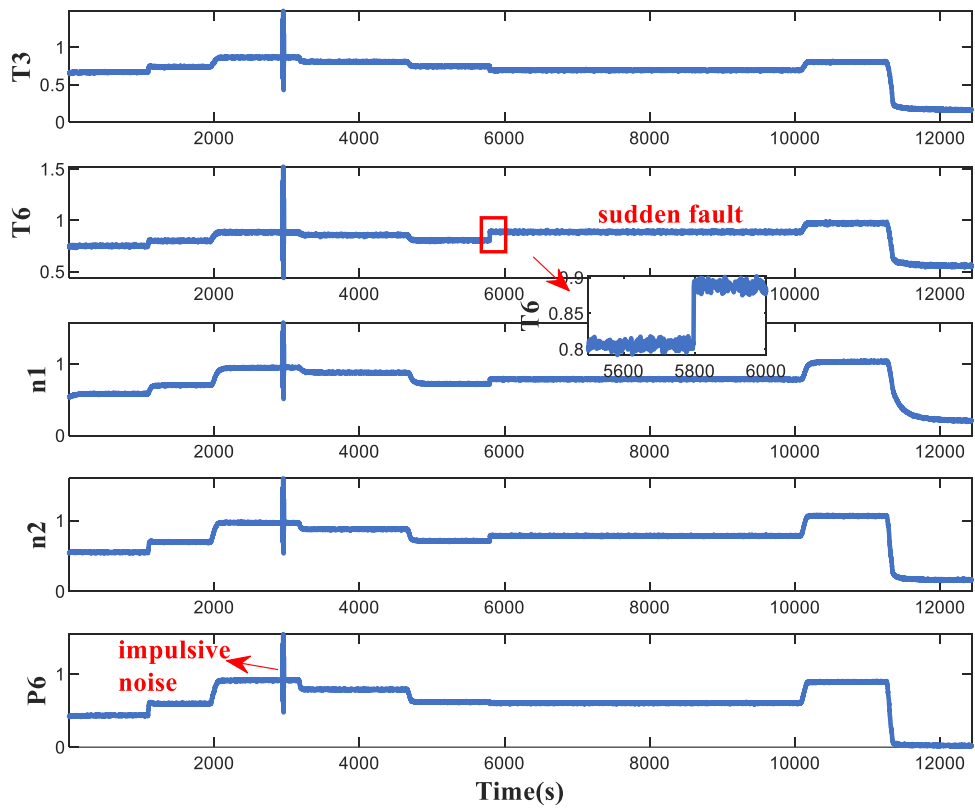


Fig. 27. Wasserstein distance of model mismatch feature distribution for gradational degradation.

of model parameters. In this process, the minimum noise criterion is established and the recursive least square method is employed to mitigate the impact of closed-loop identification. Furthermore, an enhanced form VWPAST is introduced to enhance the algorithm robustness. Both simulation and experiment data are utilized to validate the effectiveness of the established surrogate model.

The findings from the rated steady-state condition demonstrate that, with a forgetting factor of 0.995, the model exhibits moderate convergence speed and accuracy, with an MAPE of <0.0056 %. Additionally, the VWPAST is verified using steady-state data contaminated by impulsive noise, revealing enhanced robustness in identification when such impulsive occurs. The surrogate model output can effectively track the performance model output even when there are changes in operating conditions. For operating conditions, the error remains below 2.038 % and the MAPE is <0.275 %. These results demonstrate that the proposed model is applicable for gas turbines for variable operating conditions. In a gas turbine bench test, the maximum relative error between the output of the surrogate model and the measurements of the actual gas turbine is 0.549 %, and MAPE is within 0.083 %, which proves that the surrogate model certainly has value in engineering application.

The surrogate model proposed in this study exhibits great potential in the field of gas turbine condition monitoring. Based on two examples of sudden fault and gradational degradation, the results demonstrate that as the gas turbine condition changes, so does the eigenvalue of the surrogate model, indicating a corresponding alteration in its structural configuration. Wasserstein distance was used to quantify the changes of model mismatch features distribution between the normal condition and the actual gas turbine. It can be seen from the results that the model mismatch features are easier to capture in practical applications and have more general



**Fig. 28.** Operation data after implantation of impulsive noise and sudden failure.

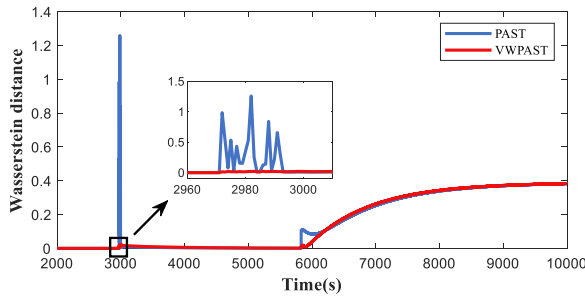


**Fig. 29.** Comparison of detection results of PAST and VW-PAST.

applicability than the changes in the model eigenvalue. In addition, compared with the PAST, VW-PAST has stronger robustness when impulsive noise occurs, and can significantly reduce the false alarm rate.

The surrogate model developed in this study is based on a linear framework and employs IHA form for online identification, ensuring both computational efficiency and high-precision results. By monitoring shifts in the surrogate model parameters, feedback from the gas turbines can be acquired for condition monitoring, which reflects the characteristics of real-time and bidirectional communication of digital twin and introduces a novel approach to the development of gas turbine digital twin. In future research, the convergence speed of the surrogate model should be examined to streamline the algorithm, enabling the model to converge more rapidly to the true value and function effectively at high sampling frequencies. Moreover, integrating prior physical knowledge about gas turbines into the model could allow it to concentrate on the evolution of one or more specific components during parameter adjustments. This enhancement would significantly improve its performance in condition monitoring.

#### CRediT authorship contribution statement

**Junqi Luan:** Writing – original draft, Methodology, Investigation, Formal analysis, Conceptualization. **Shuying Li:** Writing – review & editing, Visualization, Validation. **Yunpeng Cao:** Supervision, Project administration, Funding acquisition,

Conceptualization. **Chengzhong Gu:** Resources, Data curation.

### Declaration of competing interest

The authors declare that they have no known competing financial interests or personal relationships that could have appeared to influence the work reported in this paper.

### Data availability

The authors do not have permission to share data.

### Acknowledgment

This research was supported by the National Science and Technology Major Project (2019-I-0003–0004).

### References

- [1] U. Igie, P. Pilidis, D. Fouflias, et al., Industrial gas turbine performance: compressor fouling and on-line washing, *J. Turbomach.* 136 (2014), <https://doi.org/10.1115/1.4027747>.
- [2] M. Tahan, E. Tsoutsanis, M. Muhammad, et al., Performance-based health monitoring, diagnostics and prognostics for condition-based maintenance of gas turbines: a review, *Appl. Energy.* 198 (2017) 122–144, <https://doi.org/10.1016/j.apenergy.2017.04.048>.
- [3] A.J. Volponi, Gas turbine engine health management: past, present, and future trends, *J. Eng. Gas Turbines Power.* 136 (2014), <https://doi.org/10.1115/1.4026126>.
- [4] W. Deng, K.T.P. Nguyen, K. Medjaher, et al., Physics-informed machine learning in prognostics and health management: state of the art and challenges, *Appl. Math. Model.* 124 (2023) 325–352, <https://doi.org/10.1016/j.apm.2023.07.011>.
- [5] E.J. Tuegel, A.R. Ingraffea, T.G. Eason, et al., Reengineering aircraft structural life prediction using a digital twin, *Int. J. Aerosp. Eng.* 2011 (2011) e154798, <https://doi.org/10.1155/2011/154798>.
- [6] J. Li, G. Liu, Data-centric workshop digital twin conceptual modeling method and application, in: Proceedings of the 2022 IEEE 18th International Conference on Automation Science and Engineering (CASE), 2022, pp. 92–99, <https://doi.org/10.1109/CASE49997.2022.9926594>.
- [7] F. Tao, Q. Qi, Make more digital twins, *Nature* 573 (2019) 490–491, <https://doi.org/10.1038/d41586-019-02849-1>.
- [8] F. Tao, F. Su, A. Liu, et al., Digital twin-driven product design framework, *Int. J. Prod. Res.* 57 (2019) 3935–3953, <https://doi.org/10.1080/00207543.2018.1443229>.
- [9] E. Thirunavukarasu, R. Fang, J.A. Khan, et al., Modeling and simulation of gas turbine system on a virtual test bed (VTB), in: American Society of Mechanical Engineers Digital Collection, 2013: pp. 337–346. [10.1115/IMECE2012-8791](https://doi.org/10.1115/IMECE2012-8791).
- [10] Y.G. Li, M.F.A. Ghafir, L. Wang, et al., Nonlinear multiple points gas turbine off-design performance adaptation using a genetic algorithm, *J. Eng. Gas Turbines Power* 133 (2011), <https://doi.org/10.1115/1.4002620>.
- [11] Y.G. Li, Gas turbine performance and health status estimation using adaptive gas path analysis, *J. Eng. Gas Turbines Power* 132 (2010), <https://doi.org/10.1115/1.3159378>.
- [12] D. Huang, S. Ma, D. Zhou, et al., Gas path fault diagnosis for gas turbine engines with fully operating regions using mode identification and model matching, *Meas. Sci. Technol.* 34 (2022) 015903, <https://doi.org/10.1088/1361-6501/ac97b4>.
- [13] A.I. Abed, L.Wei Ping, Implementing data mining techniques for gas-turbine (GT) health tracking and life management: the bibliographic perspective, *Expert Syst. Appl.* 252 (2024) 124077, <https://doi.org/10.1016/j.eswa.2024.124077>.
- [14] X. Liu, Y. Chen, L. Xiong, et al., Intelligent fault diagnosis methods toward gas turbine: a review, *Chin. J. Aeronaut.* 37 (2024) 93–120, <https://doi.org/10.1016/j.cja.2023.09.024>.
- [15] Q. Yang, S. Li, Y. Cao, A new component map generation method for gas turbine adaptation performance simulation, *J. Mech. Sci. Technol.* 31 (2017) 1947–1957, <https://doi.org/10.1007/s12206-017-0344-5>.
- [16] V. Sethi, G. Doulgeris, P. Pilidis, et al., The map fitting tool methodology: gas turbine compressor off-design performance modeling, *J. Turbomach.* 135 (2013), <https://doi.org/10.1115/1.4023903>.
- [17] J. Li, Y. Ying, Gas turbine gas path diagnosis under transient operating conditions: a steady state performance model based local optimization approach, *Appl. Therm. Eng.* 170 (2020) 115025, <https://doi.org/10.1016/j.applthermaleng.2020.115025>.
- [18] Y. Ying, J. Li, An improved performance diagnostic method for industrial gas turbines with consideration of intake and exhaust system, *Appl. Therm. Eng.* 222 (2023) 119907, <https://doi.org/10.1016/j.applthermaleng.2022.119907>.
- [19] Y. Yin, Z. Wen, X. Guo, A novel method of Gas-Path health assessment based on exhaust electrostatic signal and performance parameters, *Measurement* 224 (2024) 113810, <https://doi.org/10.1016/j.measurement.2023.113810>.
- [20] F. Lu, H. Ju, J. Huang, An improved extended Kalman filter with inequality constraints for gas turbine engine health monitoring, *Aerosp. Sci. Technol.* 58 (2016) 36–47, <https://doi.org/10.1016/j.ast.2016.08.008>.
- [21] L. Alessandrini, M. Basso, M. Galanti, et al., Maximum likelihood virtual sensor based on thermo-mechanical internal model of a gas turbine, *IEEE Trans. Control Syst. Technol.* 29 (2021) 1233–1245, <https://doi.org/10.1109/TCST.2020.3003729>.
- [22] B. Pourbabae, N. Meskin, K. Khorasani, Sensor fault detection, isolation, and identification using multiple-model-based hybrid kalman filter for gas turbine engines, *IEEE Trans. Control Syst. Technol.* 24 (2016) 1184–1200, <https://doi.org/10.1109/TCST.2015.2480003>.
- [23] G.Y. Chung, J.V.R. Prasad, M. Dhingra, et al., Real time analytical linearization of turbofan engine model, *J. Eng. Gas Turbines Power* 136 (2013), <https://doi.org/10.1115/1.4025310>.
- [24] S. Tasoujian, J. Lee, K. Grigoriadis, et al., Robust linear parameter-varying output-feedback control of permanent magnet synchronous motors, *Syst. Sci. Control Eng.* 9 (2021) 612–622, <https://doi.org/10.1080/21642583.2021.1974600>.
- [25] Y. Ma, J. Liu, L. Zhu, et al., Accommodation of multishaft gas turbine switching control gain tuning problem to inlet guide vane position, *J. Eng. Gas Turb. Power* 144 (2022) 031014, <https://doi.org/10.1115/1.4052559>.
- [26] F. Lu, J. Qian, J. Huang, et al., In-flight adaptive modeling using polynomial LPV approach for turbofan engine dynamic behavior, *Aerosp. Sci. Technol.* 64 (2017) 223–236, <https://doi.org/10.1016/j.ast.2017.02.003>.
- [27] M.G.D. Giorgi, S. Campilongo, A. Ficarella, A diagnostics tool for aero-engines health monitoring using machine learning technique, *Energy Procedia* 148 (2018) 860–867, <https://doi.org/10.1016/j.egypro.2018.08.109>.
- [28] B. Li, Y.P. Zhao, Y.B. Chen, Learning transfer feature representations for gas path fault diagnosis across gas turbine fleet, *Eng. Appl. Artif. Intell.* 111 (2022) 104733, <https://doi.org/10.1016/j.engappai.2022.104733>.

- [29] M. Bai, J. Liu, J. Chai, et al., Anomaly detection of gas turbines based on normal pattern extraction, *Appl. Therm. Eng.* 166 (2020) 114664, <https://doi.org/10.1016/j.aplthermaleng.2019.114664>.
- [30] X. Yang, M. Bai, J. Liu, et al., Gas path fault diagnosis for gas turbine group based on deep transfer learning, *Measurement* 181 (2021) 109631, <https://doi.org/10.1016/j.measurement.2021.109631>.
- [31] Z. Zhou, W. Zhang, P. Yao, et al., More realistic degradation trend prediction for gas turbine based on factor analysis and multiple penalty mechanism loss function, *Reliab. Eng. Syst. Saf.* 247 (2024) 110097, <https://doi.org/10.1016/j.ress.2024.110097>.
- [32] K. Cheng, K. Zhang, Y. Wang, et al., Research on gas turbine health assessment method based on physical prior knowledge and spatial-temporal graph neural network, *Appl. Energy* 367 (2024) 123419, <https://doi.org/10.1016/j.apenergy.2024.123419>.
- [33] Y. Zhang, Y. Xin, Z. Liu, et al., Health status assessment and remaining useful life prediction of aero-engine based on BiGRU and MMoE, *Reliab. Eng. Syst. Saf.* 220 (2022) 108263, <https://doi.org/10.1016/j.ress.2021.108263>.
- [34] X. Cheng, H. Zheng, Q. Yang, et al., Surrogate model-based real-time gas path fault diagnosis for gas turbines under transient conditions, *Energy* 278 (2023) 127944, <https://doi.org/10.1016/j.energy.2023.127944>.
- [35] V. Zaccaria, A.D. Fentaye, K. Kyriyanidis, Assessment of dynamic bayesian models for gas turbine diagnostics, part 1: prior probability analysis, *Machines* 9 (2021) 298, <https://doi.org/10.3390/machines9110298>.
- [36] D. van der Hoek, M. Sinne, E. Simley, et al., Estimation of the ambient wind field from wind turbine measurements using gaussian process regression, in: *Proceedings of the 2021 American Control Conference (ACC)*, 2021, pp. 558–563, <https://doi.org/10.23919/ACC50511.2021.9483088>.
- [37] Z. Sun, R. Zhang, X. Zhu, The progress and trend of digital twin research over the last 20 years: a bibliometrics-based visualization analysis, *J. Manuf. Syst.* 74 (2024) 1–15, <https://doi.org/10.1016/j.jmssy.2024.02.016>.
- [38] J. Sun, Z. Yan, Y. Han, et al., Deep learning framework for gas turbine performance digital twin and degradation prognostics from airline operator perspective, *Reliab. Eng. Syst. Saf.* 238 (2023) 109404, <https://doi.org/10.1016/j.ress.2023.109404>.
- [39] M. Hu, Y. He, X. Lin, et al., Digital twin model of gas turbine and its application in warning of performance fault, *Chin. J. Aeronaut.* 36 (2023) 449–470, <https://doi.org/10.1016/j.cja.2022.07.021>.
- [40] J. Zhang, Z. Wang, S. Li, et al., A digital twin approach for gas turbine performance based on deep multi-model fusion, *Appl. Therm. Eng.* 246 (2024) 122954, <https://doi.org/10.1016/j.aplthermaleng.2024.122954>.
- [41] Y. Ma, X. Zhu, J. Lu, et al., Construction of data-driven performance digital twin for a real-world gas turbine anomaly detection considering uncertainty, *Sensors* 23 (2023) 6660, <https://doi.org/10.3390/s23156660>. -Basel.
- [42] Z. Wang, Y. Wang, X. Wang, et al., A novel digital twin framework for aeroengine performance diagnosis, *Aerospace* 10 (2023) 789, <https://doi.org/10.3390/aerospace10090789>.
- [43] X. Zhao, M.H. Dao, Q.T. Le, Digital twining of an offshore wind turbine on a monopile using reduced-order modelling approach, *Renew. Energy* 206 (2023) 531–551, <https://doi.org/10.1016/j.renene.2023.02.067>.
- [44] S. Chakraborty, S. Adhikari, R. Ganguli, The role of surrogate models in the development of digital twins of dynamic systems, *Appl. Math. Modell.* 90 (2021) 662–681, <https://doi.org/10.1016/j.apm.2020.09.037>.
- [45] W. Bartelmus, R. Zimroz, A new feature for monitoring the condition of gearboxes in non-stationary operating conditions, *Mech. Syst. Signal Process.* 23 (2009) 1528–1534, <https://doi.org/10.1016/j.ymssp.2009.01.014>.
- [46] W. Bartelmus, R. Zimroz, Vibration condition monitoring of planetary gearbox under varying external load, *Mech. Syst. Signal Process.* 23 (2009) 246–257, <https://doi.org/10.1016/j.ymssp.2008.03.016>.
- [47] R. Zimroz, W. Bartelmus, T. Barszcz, et al., Diagnostics of bearings in presence of strong operating conditions non-stationarity—A procedure of load-dependent features processing with application to wind turbine bearings, *Mech. Syst. Signal Process.* 46 (2014) 16–27, <https://doi.org/10.1016/j.ymssp.2013.09.010>.
- [48] E. Ceci, Y. Shen, G.B. Giannakis, et al., Graph-Based Learning Under Perturbations via Total Least-Squares, *IEEE Trans. Signal Process.* 68 (2020) 2870–2882, <https://doi.org/10.1109/TSP.2020.2982833>.
- [49] W. Gui, J. Gao, C. Yang, et al., Optimized FCS-MPCC based on disturbance feedback rejection for IPMSMs under demagnetization fault in high-speed trains, *Control Eng. Pract.* 141 (2023) 105670, <https://doi.org/10.1016/j.conengprac.2023.105670>.
- [50] L. Shen, Y. Zakharov, M. Niedźwiecki, et al., Finite-window RLS algorithms, *Signal Process* 198 (2022) 108599, <https://doi.org/10.1016/j.sigpro.2022.108599>.
- [51] Z. Chen, H. Fang, Data-driven fault detection and isolation inspired by subspace identification method, in: *Proceedings of the 33rd Chinese Control Conference*, 2014, pp. 3322–3327, <https://doi.org/10.1109/ChiCC.2014.6895489>.
- [52] C. Djeddi, A. Hafaifa, A. Iratni, et al., Robust diagnosis with high protection to gas turbine failures identification based on a fuzzy neuro inference monitoring approach, *J. Manuf. Syst.* 59 (2021) 190–213, <https://doi.org/10.1016/j.jmssy.2021.02.012>.
- [53] X. Rong, V. Solo, State space subspace noise modeling with guaranteed stability, in: *Proceedings of the 2023 62nd IEEE Conference on Decision and Control (CDC)*, 2023, pp. 4203–4208, <https://doi.org/10.1109/CDC49753.2023.10383942>.
- [54] X. Lu, M. Cannon, Robust adaptive model predictive control with persistent excitation conditions, *Automatica* 152 (2023) 110959, <https://doi.org/10.1016/j.automatica.2023.110959>.
- [55] I. Markovsky, E. Prieto-Araujo, F. Dörfler, On the persistency of excitation, *Automatica* 147 (2023) 110657, <https://doi.org/10.1016/j.automatica.2022.110657>.
- [56] O. Mohamed, D. Younis, H. Abdelwahab, et al., Comparative study between subspace method and prediction error method for identification of gas turbine power plant, in: *Proceedings of the 2014 6th International Congress on Ultra Modern Telecommunications and Control Systems and Workshops (ICUMT)*, IEEE, St. Petersburg, Russia, 2014, pp. 421–428, <https://doi.org/10.1109/ICUMT.2014.7002138>.
- [57] O. Mohamed, J. Wang, A. Khalil, et al., Predictive control strategy of a gas turbine for improvement of combined cycle power plant dynamic performance and efficiency, *Springerplus* 5 (2016) 980, <https://doi.org/10.1186/s40064-016-2679-2>.
- [58] W. Favoreel, B. De Moor, P. Van Overschee, Subspace state space system identification for industrial processes, *J. Process Control.* 10 (2000) 149–155, [https://doi.org/10.1016/S0959-1524\(99\)00030-X](https://doi.org/10.1016/S0959-1524(99)00030-X).
- [59] A. Goel, D.S. Bernstein, A Targeted Forgetting Factor for Recursive Least Squares, in: *Proceedings of the 2018 IEEE Conference on Decision and Control (CDC)*, 2018, pp. 3899–3903, <https://doi.org/10.1109/CDC.2018.8619181>.
- [60] L. Shan, H. Chen, J. Luan, et al., Application of adaptive forgetting factor RLS algorithm in target tracking, in: *Proceedings of the 2017 Chinese Automation Congress (CAC)*, 2017, pp. 1838–1843, <https://doi.org/10.1109/CAC.2017.8243067>.
- [61] B. Yang, Projection approximation subspace tracking, *IEEE Trans. Signal Process.* 43 (1995) 95–107, <https://doi.org/10.1109/78.365290>.
- [62] A.G. Costa Junior, J.A. Riul, P.H.M. Montenegro, Application of the subspace identification method using the N4SID technique for a robotic manipulator, *IEEE Lat. Am. Trans.* 14 (2016) 1588–1593, <https://doi.org/10.1109/TLA.2016.7483487>.
- [63] S. Xiang, F. Nie, C. Zhang, Learning a Mahalanobis distance metric for data clustering and classification, *Pattern Recognit.* 41 (2008) 3600–3612, <https://doi.org/10.1016/j.patcog.2008.05.018>.
- [64] F. Liyun, S. Chongchong, L. Zhongyang, et al., Multi-objective optimization of three-shaft gas turbine for sudden unloading, *IFAC Pap.* 54 (2021) 400–405, <https://doi.org/10.1016/j.ifacol.2021.10.195>.
- [65] X. Pu, S. Liu, H. Jiang, et al., Adaptive gas path diagnostics using strong tracking filter, *Proc. Inst. Mech. Eng. G J. Aerosp. Eng.* 228 (2014) 577–585, <https://doi.org/10.1177/0954410013478514>.
- [66] J. Luan, Y. Cao, R. Ao, et al., A new health evaluation approach for gas turbine using its component performance parameters, in: *American Society of Mechanical Engineers Digital Collection*, 2022. [10.1115/GT2022-83233](https://doi.org/10.1115/GT2022-83233).

- [67] J. Gao, K. Yang, M. Shen, et al., Data-driven traffic sensor location and path flow estimation using wasserstein metric, *Appl. Math. Modell.* 133 (2024) 211–231, <https://doi.org/10.1016/j.apm.2024.05.021>.
- [68] Y. Cao, L. Chen, J. Du, et al., The degradation simulation of compressor salt fog fouling for marine gas turbine, in: American Society of Mechanical Engineers Digital Collection, 2017. [10.1115/GT2017-64464](https://doi.org/10.1115/GT2017-64464).
- [69] A.P. Tarabrin, V.A. Schurovsky, A.I. Bodrov, et al., An analysis of axial compressors fouling and a cleaning method of their blading, in: American Society of Mechanical Engineers Digital Collection, 2015. [10.1115/96-GT-363](https://doi.org/10.1115/96-GT-363).